Construction and Building Materials 416 (2024) 135175

Contents lists available at ScienceDirect

Construction and Building Materials

journal homepage: www.elsevier.com/locate/conbuildmat

Comprehensive analysis of experimental and numerical results of bond strength and mechanical properties of fly ash based GPC and OPC concrete

Yuksel Gul Aslanbay [a], Huseyin Hilmi Aslanbay [a,*,1], Ahmet Özbayrak [a], Hurmet Kucukgoncu [b], Oguzhan Atas [c]

[a] Erciyes University, Engineering Faculty, Civil Engineering Department, Kayseri, Turkey
[b] Abdullah Gül University, Engineering Faculty, Civil Engineering Department, Kayseri, Turkey
[c] Alanya Alaaddin Keykubat University, Engineering Faculty, Civil Engineering Department, Antalya, Turkey

ARTICLE INFO

Keywords:
Geopolymer concrete
Low calcium fly ash
Pull-out test
Bond strength
Finite element method

ABSTRACT

Nowadays, materials in the more environmentally friendly waste product class, which can be an alternative to standard Portland cement (OPC), are frequently used by researchers in concrete production. One of these, namely fly ash-based geopolymer concrete (GPC), should demonstrate its superiority over OPC in terms of chemical and mechanical properties to enhance its utilization. One of the mechanical properties of GPC is the bond strength between reinforcement and concrete. In this study, it was aimed to obtain bond strengths by performing tensile tests on GPC samples with varying sodium silicate/sodium hydroxide (SS/SH) and alkaline activator/fly ash (AA/FA) ratios. A pull-out experimental setup was prepared in accordance with RILEM Standard. Experimental results were compared with numerical results obtained from finite element models designed in ABAQUS software and were found to be compatible. When evaluated in terms of peak load and max bond stress values, GPC is superior to OPC. Compared to OPC an increase in the SS/SH ratio enhances mechanical properties such as compressive strength and bond load, whereas an increase in the AA/FA ratio with a value of 0.7 in the series has the opposite effect. In the finite element models, stress values are higher in samples with an AA/FA ratio of 0.5 compared to other ratios. An increase in the AA/FA ratio leads to a decrease in stress values. The analytical results are demonstrated that the proposed model can be utilized to assess the bond strength performance between traditional reinforced concrete and fly ash-based geopolymer concrete. Additionally, as a result of experimental studies, a formula that can be used to estimate bond strength based on GPC compressive strength and shows the superiority of GPC compared to studies in the literature has been proposed.

1. Introduction

In this era, offering alternatives that are environmentally friendly and energy-efficient to traditional building materials is crucial for the future of the planet. Ordinary Portland Cement (OPC) is used as the primary binder most commonly used in traditional concrete production. Due to the widespread use of cement, there is a significant release of CO^2 into the environment during its production. In 2021, the global cement industry emitted 104 million tons of CO^2, which accounts for approximately 7.4% of all human-caused CO^2 emissions [1]. Geopolymer concretes (GPC), which can be preferred as alternatives to cement, offer the benefit of reducing CO2 emissions to the environment while also providing a way to utilize fly ashes, a hazardous waste material produced from the combustion of coal in thermal power plants[2]. In 2011, approximately 30% of the world's electricity was obtained by burning coal, and this rate is expected to be approximately 46% by 2030 [3]. Due to the increasing energy demand, the rising use of coal led to the generation of 500 million tons of fly ash in 2005, a number that reached 750 million tons by 2015 [4–6]. In summary, GPC is recognized for its advantages such as sustainability, longer service life, low carbon emissions, recycled industrial waste, and high durability [7,8]. Transforming this waste is critical for environmental conservation and sustainability [9–12].

When investigating the conducted studies, to discuss the principle of reinforced concrete behavior, which involves the collaboration of concrete and steel reinforcement, it is essential for there to be high

* Corresponding author.
E-mail address: aslanbay@erciyes.edu.tr (H.H. Aslanbay).
[1] ORC ID: 0000-0001-9739-4699

https://doi.org/10.1016/j.conbuildmat.2024.135175
Received 7 November 2023; Received in revised form 5 January 2024; Accepted 23 January 2024
Available online 1 February 2024

adherence between the concrete and the reinforcement. Hence, investigating the adherence behavior between geopolymer concrete and reinforcement is crucial for considering the use of GPC as an alternative to OPC in reinforced concrete structures [13,14]. There are studies in the literature to evaluate the bond properties between geopolymer concrete and reinforcement. However, there are very few studies in the literature investigating the bond between GPC and reinforcement, especially based on low calcium fly ash [15–17]. In their study, Jiang, Zhang et al. (2020) conducted research on geopolymer samples produced using low-calcium fly ash. They performed loading using a procedure compliant with ASTM C900 standard and investigated the bond strength. Throughout the test, the loading rate was maintained at 3 mm/min. The diameter of the used reinforcement was 0.148 in., and the embedment length was set at the sample height of 2 in. [18]. As a result, it was observed that the residual bond strength maintains a consistent relationship with the compressive strength variation. Castel and Foster (2015) conducted a study using low-calcium fly ash, subjecting 100×100×100 mm samples to the standard RILEM pull-out test. In accordance with RILEM standards, they set the total length of the sample at 120 mm for a bond length of L = 60 mm. The diameter of the reinforcement was 12 mm. The loading rate for all specimens was 0.1 kN/s. For an equivalent compressive strength, it was observed that the bond strength of geopolymer concrete was slightly better than that of the reference OPC concrete; an average increase of around 10% in bond strength was noted. Jiang, Xiao et al. (2020) produced samples with a diameter of 1 in. and a height of 2 in. to analyze the bond strength of geopolymer concrete produced from fly ash in their study, and performed the bond (adherence) test with a loading speed of 3 mm/min according to the ASTM C900 standard. The used reinforcement diameter was 0.148 in., and the embedment length was taken as the sample height. As a result of the experiment, the bond strength of GPC was higher than that of OPC [19]. In general, while exhibiting behavior similar to OPC under the same test parameters, GPC demonstrates higher bond strength [12,20]. Albidah [21] also confirmed that concrete embedded in geopolymer concrete possessed higher bond strength compared to traditional concrete. In an experiment presented by Trabacchin et al. [22], it was reported that the diameter of the reinforcement and the bond length have a significant impact on bond strength. However, there is a limited number of studies that address the variation in mixture content in geopolymer concrete. Therefore, this study aims to investigate how changes in the SS/SH ratio and the AA/FA ratio influence the bond strength. Previous studies utilized experimental methods such as pull-out tests, beam end tests, beam anchorage tests, and splice tests [23] to determine bond strength [24]. In this study, the pull-out test method was employed to determine bond strength due to its convenience during both the manufacturing phase and the execution of the experiment [25]. The experiment was conducted following the RILEM-7–11-128 standard [26]. Researchers like Al-Azzawi et al. [27], Farhan et al. [28], Castel and Foster [12], Zhao et al. [29] and Topark-Ngarm et al. [30] utilized this test method in their studies on geopolymer concrete.

In addition to experimental studies, limited research has also revealed numerical analyses to examine bond strength [31,32]. Firstly, models were presented to deal with the adherence behavior of geopolymer concrete. These proposed models were utilized in finite element modeling to validate experimental results and investigate the distribution of bond strength along the embedment length [33]. For this purpose, Le et al. [34] investigated the bond strength on geopolymer concrete samples with 12, 16 and 20 mm reinforcements using F class fly ash in their study. The experimental method employed was the pull-out test. The ABAQUS software was used for finite element analysis. It was informed that an increase in concrete compressive strength leads to a significant increase in bond strength. Additionally, it was concluded that the thickness of the concrete cover affects the bond strength. In another study [25], analysis was made using ABAQUS finite element (FE) code. The interface between geopolymer concrete and reinforcement was modeled by Rolland et al. [25] using cohesive elements associated with the previously defined analytical bond-slip law.

A strong bond between reinforcement and concrete is of critical importance for the structural integrity and durability of buildings. A robust bond ensures that structural elements of a building are strongly interconnected, thereby enhancing the structure's resilience against external forces such as wind, earthquakes, and loads as well as potential deterioration over time. The aim of this study is to investigate the bond between fly ash-based geopolymer concrete and ribbed reinforcement steel, both experimentally and numerically. The pull-out test method was applied in this experimental study. The test results were compared with the performance of the reference OPC specimens. The notable aspect of this study is its expansion beyond experimental investigations by incorporating numerical analyses. This extension allows for a comprehensive exploration of the contributions of geopolymer concrete (GPC) usage in terms of bond stress compared to Ordinary Portland Cement (OPC) concrete usage. The study also includes intra-comparisons of GPC samples, enabling the determination of the impact of the considered mixture proportions on mechanical properties. During tests, the occurrence of the collapse mechanism in the samples takes place in various ways. These situations manifest as the termination of the experiment due to debonding of the reinforcement or the splitting of the concrete specimen without the detachment of the reinforcement. When considering the failure mode parameter of the bond between reinforcement and concrete, variations according to mixture proportions were observed. Furthermore, within the scope of finite element analyses, the models' damage distributions, stress distributions, and plastic deformation graphs were incorporated to facilitate a comprehensive evaluation of GPC and OPC samples. Through both experimental and numerical investigations, bond stress-slip curves were obtained, enabling the determination of crucial criteria for comparing GPC and OPC samples based on load-bearing capacity and displacement data. This study presents an equation to be used in calculating the adhesion strength based on compressive strength (fc) for GPC made with fly ash, a waste product class that shows superior adhesion strength than OPC.

1.1. Research significance

The experimental study put forward in this article is designed to develop advanced materials for a sustainable industry focusing on the reuse of raw material waste [35]. These low-cost waste materials would not only provide a reduction in the total cost of final products but would also provide significant energy savings because they do not contain cement. For this reason, geopolymer concrete was used within the scope of the study. It was investigated whether GPC could be an alternative to cement-added concrete. The fresh and hardened properties of the GPC mixture and the parameters affecting it must be well understood before practical application. Therefore, it is important to conduct comprehensive studies in which all important parameters are taken into account in order to collect a significant amount of information about the material and disseminate this relatively new material technology into fields and field applications [36].

In addition, GPC provides similar or even higher physical-mechanical performance than conventional concrete. One of these mechanical properties is undoubtedly adherence strength, which enables concrete and reinforcement to work together. The bond strength affects the anchorage length of the reinforcement at the ultimate limit state and controls the tension stiffness, crack spacing, and width of the structural member at the service limit state [37,38]. For this reason, it was investigated how this bond changes at different Sodium Silicate/Sodium Hydroxide (SS/SH) and alkaline activator/fly ash (AA/FA) ratios.

In addition, analytical studies to reveal adherence strength are quite limited and more studies are needed to be validated by reference. Therefore, the main aim of the study is to expand the knowledge in these fields both experimentally and analytically in order to promote the use of this material for structural applications by contributing to the

Table 1
Chemical components of fly ash.

Components	%
SiO_2, 1	55.9
Al_2O_3, 2	20.7
Fe_2O_3, 3	9.31
Sum of 1, 2, 3	85.9
CaO	3.98
MgO	2.33
SO_3	0.33
Na_2O	1,35
K_2O	2.19
Cl-	0.05
LOI (loss of ignition)	2.22
Fineness (>45 μm)	17.4

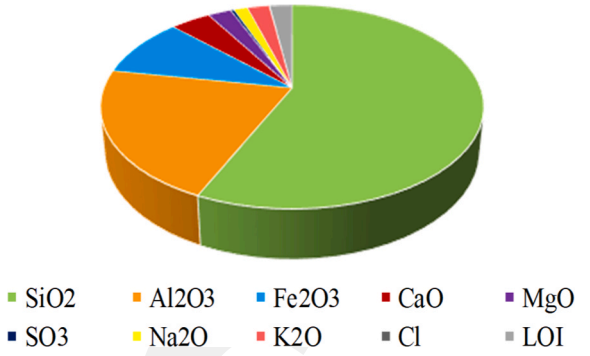

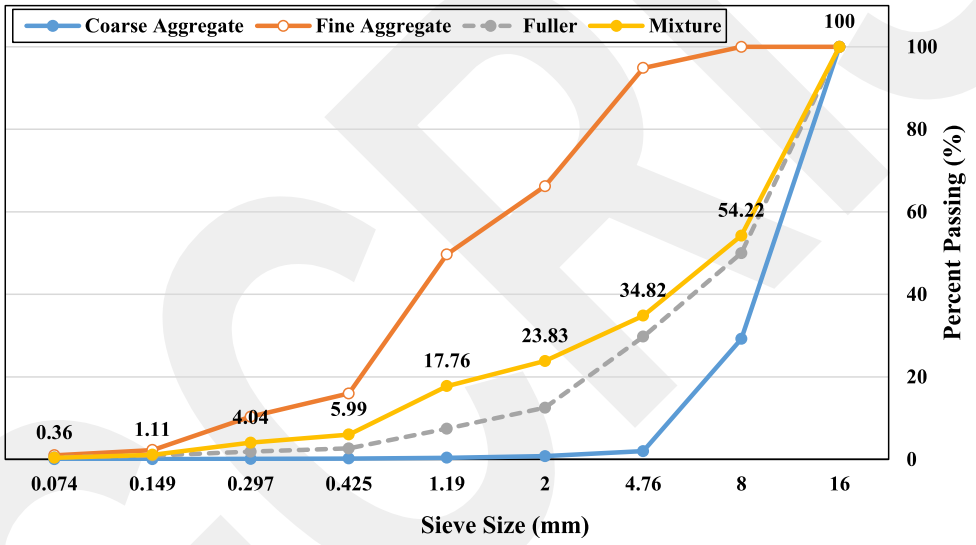

Fig. 1. Grading curve for aggregates D_{max}= 16 mm.

evaluation of design indicators.

2. Experimental program

2.1. Materials

Low-calcium fly ash (FA) obtained from Adana, İsken Sugözü Power Plant was utilized for the production of geopolymer concrete (GPC). The chemical components of the fly ash-based aluminosilicate used in the study are shown in Table 1. For the used FA to fall within the low-carbon fly ash class according to ASTM C618 [39], the total SiO_2, Al_2O_3, and Fe_2O_3 ratio must be greater than 70%. It is also seen in Table 1 that the sum of these three oxides is 85.9% and is in the F class fly ash class. The reaction performance of FA is affected by several factors such as the fineness of the material, the percentage of reactive silica, and the quality of the coal used to obtain the waste. The color of the fly ash is dark green and its specific gravity is 2.32 g/cm^3, measured using the Blaine Air Permeability method [40].

Although potassium-based activators are also used in the geopolymerization process, the most preferred alkali activators are sodium hydroxide (NaOH) and sodium silicate (Na_2SiO_3). The chemical reactions of the geopolymer matrix are dependent on the molarities of NaOH and Na_2SiO_3 present in the alkali activator solution. Due to the presence of readily reactive dissolved silicon particles during the geopolymerization process, Na_2SiO_3 solution exhibits a higher activation potential along with NaOH. NaOH grains in pallet form used to prepare sodium hydroxide solution (14 M) are 98% pure. After the NaOH solution was prepared, it was kept at room temperature for at least 24 h before being used. The proportions of the components in the Na_2SiO_3 solution are Na_2O = 14.41%, SiO_2 = 29.64%, H_2O = 55.73% and the bulk density is 1510 kg/m^3. Crushed stone with a diameter of 7–14 mm was used as coarse aggregate, while river sand with a diameter of 0.3 mm was used as fine aggregate. The gradation curves of the aggregates are shown in Fig. 1. In order to minimize the absorption of water and chemicals, the moisture content of the aggregates was adjusted to achieve a saturated surface-dry state.

Table 2
Formulations and mixture quantities for the experimental samples (kg/m^3).

Sample No	Sample Name	FA	SS	SH	Fine Aggregate	Coarse Aggregate	SS/SH	AA/FA
1	A1.5W0.5	406	122	81	643	1194	1.5	0.5
2	A1.5W0.6	406	146	97	643	1194	1.5	0.6
3	A1.5W0.7	406	171	114	643	1194	1.5	0.7
4	A2.5W0.5	406	145	58	643	1194	2.5	0.5
5	A2.5W0.6	406	174	70	643	1194	2.5	0.6
6	A2.5W0.7	406	203	81	643	1194	2.5	0.7
7	A3.5W0.5	406	158	45	643	1194	3.5	0.5
8	A3.5W0.6	406	189	54	643	1194	3.5	0.6
9	A3.5W0.7	406	221	63	643	1194	3.5	0.7

FA: Fly Ash, SS: Sodium Silicate Solution (Na_2SiO_3), SH: Sodium Hydroxide Solution (NaOH), AA: NaOH+Na_2SiO_3

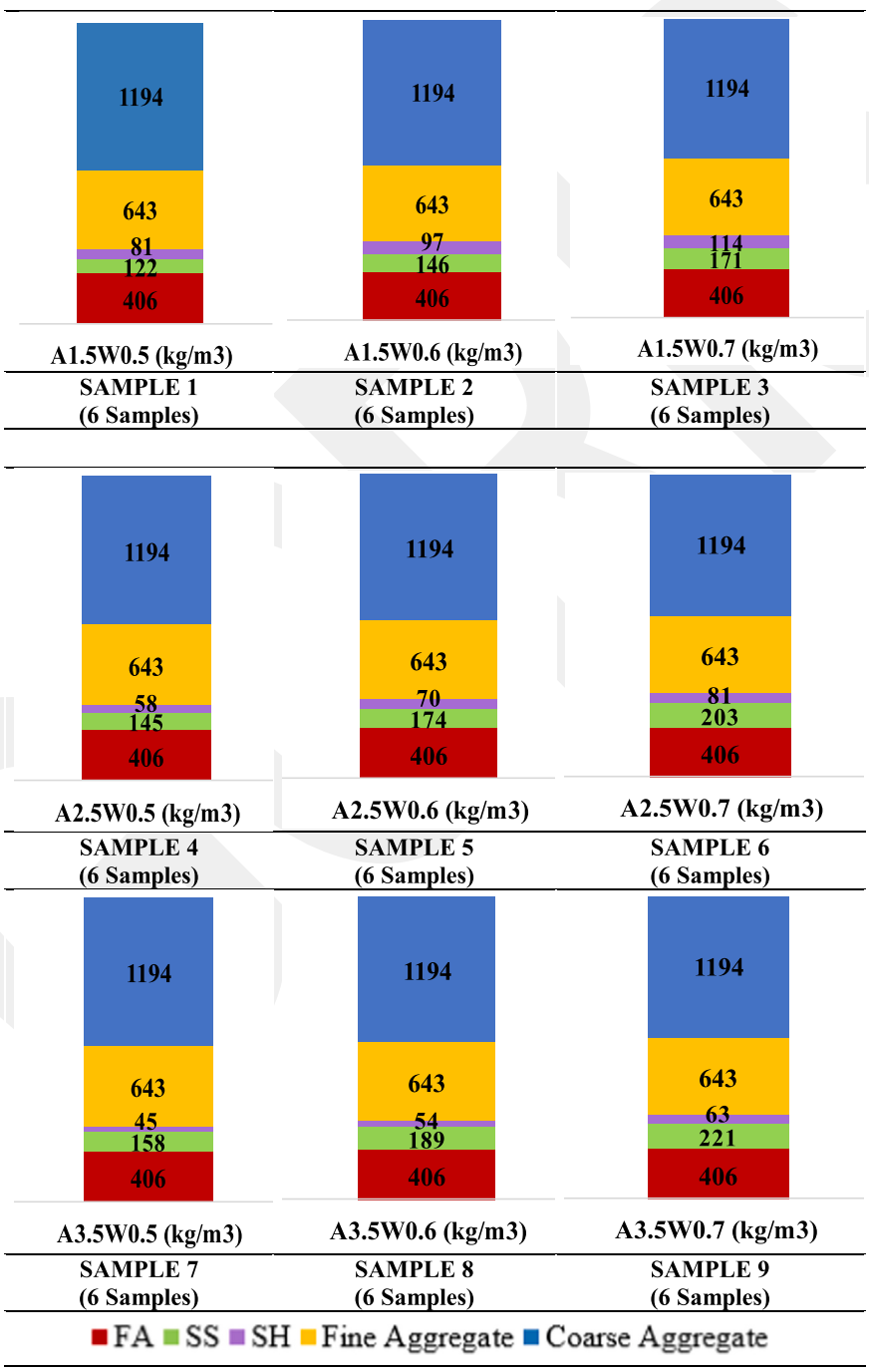

Fig. 2. Mix proportions for pull-out test for 54 samples.

Fig. 3. Placement of the reinforcements.

Table 3
Ordinary Portland Cement based concrete mix.

Materials	OPC (kg/m^3)
Cement CEM I 52.5 N CE CP2 NF	372
Sand	767
Coarse Aggregate	465
Fine Aggregate	652
Total Water	156

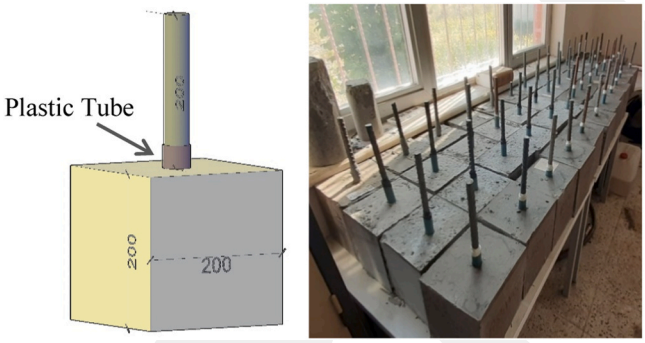

Fig. 4. Schematic representation of samples and post-production view.

2.2. Mix proportions

The most common activator used for preparing GPC is a combination of $NaSi_2O_3$ and NaOH. The activators have a significant impact on the polymerization process. When the alkali activator dissolves Si and Al from the binding material to form the matrix, polymerization occurs to a high degree. The activator prepared using NaOH and Na_2SiO_3 enhances the reactivity of FA. Therefore, the amounts of alkaline activators should be carefully adjusted when designing the GPC mix [41,42]. The formulations with different alkali activator ratios used in the study are given in Table 2.

A total of 54 cubic samples with dimensions of 200×200×200 mm were produced, with 6 samples from each of the 9 different mixtures. These mixtures had SS/SH ratios of 1.5, 2.5, and 3.5, as well as AA/FA ratios of 0.5, 0.6, and 0.7. Fig. 2 depicts the schematic distribution of the samples. In the sample designations, the term "A" indicates the SS/SH ratio, while "W" indicates the AA/FA ratio.

2.3. Mixing and casting

An apparatus shown in Fig. 3 was designed and fabricated to ensure that the reinforcements could remain in an upright position during the concrete casting process without being affected by the concrete pouring. The reinforcements were placed in the molds with the help of the setup and made ready for concrete casting. For the production of geopolymer concrete mortar, firstly, coarse and coarse aggregate with saturated dry surface and ash were mixed for 2 min. After the entire solution of Na_2SiO_3 from the alkali activators was poured into the mixture, the NaOH solution prepared 24 h before it was added to the mixture slowly for 5 min [7,8]. After 8 min in total, no extra water or plasticizer was added to the concrete mix. The samples to be subjected to the pull-out test were placed in the cube molds by skewering in two stages just after the concrete was poured. Each of the test samples given in Table 2 were produced in 6 pieces and 3 were used in compressive tests and 3 in bond tests.

2.4. Curing procedure

The concrete samples were subjected to thermal curing by heating them at 90 °C for 24 h in an oven [43,44]. Afterwards, the samples removed from the molds were stored at room temperature for 28 days until strength tests. OPC samples were cured by wet curing for 28 days.

2.5. OPC-based concrete as reference samples

For the purpose of comparing and assessing the mechanical properties and performance of geopolymer concrete, reference samples of Ordinary Cement (OPC) based concrete adherence specimens were produced and labeled as OPC. The material quantities for the OPC concrete mixture are presented in Table 3.

2.6. Testing program

To determine the mechanical properties of hardened concrete, compressive strength tests were conducted on 200×200×200 mm cubic samples. The compressive strength tests were carried out in accordance with ASTM C39 standards [45]. Additionally, the elastic modulus of the cubic samples was determined according to ASTM standard C469M-14 since it was an important mechanical property indicating the linear strength of the concrete material [46]. Utilizing the samples shown in Fig. 4, a standard RILEM pull-out test was conducted to investigate the bond between reinforcement and geopolymer concrete.

The recent experimental studies conducted using this testing method consistently demonstrate that geopolymers generally exhibit a strong bond performance with reinforcements [10,15,20]. B420C class ribbed reinforcement with a diameter of 16 mm was used in the bond test samples. The experiments utilized the RILEM [26] standard, and previous studies conducted in accordance with RILEM guidelines were provided guidance for the design of the specimen and the experimental

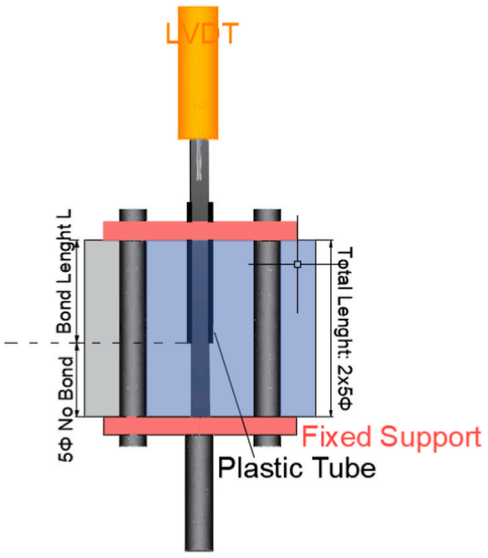

Fig. 5. Pull-out test according to standard recommendations.

setup shown in Fig. 5 [35,47,48]. An adhesive surface of 80 mm in length, extending 5 times the diameter of the reinforcement from the base of the cubic specimen, was formed. Following this, the upper portion of the exposed reinforcement was covered with a plastic tube to prevent contact with the concrete [26,49]. The plastic tube was extended beyond the concrete sample by 30 mm, encompassing the reinforcement.

To conduct the bond tests, a steel apparatus was fabricated in accordance with the dimensions of the 200×200×200 samples, as illustrated in Fig. 6. The produced apparatus consisted of two plates and four studs. The adherence specimen was compressed between the two plates. A circular hole was left at the center of the upper plate to allow the bond reinforcement to pass through. A cylindrical steel rod was welded to the bottom plate to securely hold the profile of the pull-out test apparatus and allow the specimen to be subjected to the load. This enables the specimen to be exposed to the force while the profile remains fixed. After the adherence sample was placed, the shafts were fixed with nuts so that the concrete was compressed between the plates.

Bond tests were carried out with the help of the setup prepared in the tensile test device shown in Fig. 7. Three Linear Variable Displacement Transducers (LVDT) were used to measure displacements in the experiments. The bottom LVDT was used to check for pull-out in the lower vice, while the middle LVDT was used to check for any elongation between the assembly shafts. The upper LVDT provides the measurement of the total distance traveled control. The load cell utilized in the tensile testing machine was used to measure the applied force. By connecting the load cell and three LVDT data loggers, experimental data was collected. A loading rate of 0.75 kN/s was set for all specimens. The reinforcements were subjected to the test after a 28-day curing period. A total of 30 pull-out tests were conducted, consisting of 27 geopolymer concrete specimens and 3 OPC concrete specimens. In the experimental study, the final bond stress was calculated by using Eq. 1[12,26].

$$\tau_u = \frac{F_{\max}}{\pi.\varnothing.L} \quad (1)$$

where, the ultimate bond stress is τ_u, $\varnothing$ is the diameter of the reinforcement, L is the bond length and F_{max} is the ultimate tensile force.

3. Analytical method

The finite element models of adherence samples within the scope of the analytical approach were performed using the ABAQUS [50] software. In order to enable nonlinear analysis, the Dynamic Explicit method was employed as the approach. The modeling was conducted

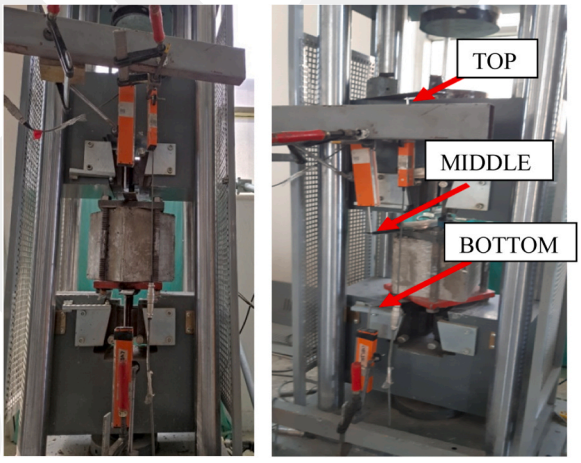

Fig. 7. Bond test setup.

Fig. 6. Steel apparatus and schematic illustration used in bond tests.

Table 4
CDP parameters for ABAQUS material definition of concrete.

Parameter	Taken value	Description
φ	50	Dilation angle
ϵ	0.1	Eccentricity
f_{b0}/f_{c0}	1.16	The ratio of initial equibiaxial compressive yield stress to initial uniaxial compressive yield stress.
K	0.6667	K_c, the ratio of the second stress invariant on the tensile meridian
υ	0.01	Viscosity parameter

using the SI unit system. In the numerical modeling of the samples, material models were designed taking into account nonlinear behavior, incorporating plastic behaviors for analysis. The Concrete Damaged Plasticity (CDP) material model, which was a concrete damaged plasticity model, was employed for concrete. The CDP model utilizes isotropic tensile and compressive plasticity along with the concept of isotropic damaged elasticity to represent the inelastic behavior of concrete [51,52]. The parameters of the CDP (Concrete Damaged Plasticity) model were derived from laboratory compression and splitting test results of concrete obtained from cylindrical specimens used in the production of adherence samples. The stress-strain curve obtained from the compression test was modified within the framework of the CDP model and defined in the software. The CDP model greatly contributes to realistically describing the damage mechanisms and crack development of concrete under loading. Some of the parameters used within the scope of the CDP model are provided in Table 4. Different CDP models were defined in the software for each distinct geopolymer adherence sample, and individual analyses were conducted for each type. Additionally, a model was defined for the adherence sample produced with Ordinary Portland Cement (OPC), and a comparison was made. 2.35 g/cm^3 was entered as the concrete unit volume weight for all samples.

f_{b0}/f_{c0} is the ratio of biaxial compressive strength to uniaxial compressive strength and the default value 1.16 in ABAQUS[53]. The K value is used to define the shape of the failure surface in the deviatoric plane which is the ratio of the second stress invariant for compression and tension at the same hydrostatic stress, υ is the viscosity parameter which allows the stresses to move beyond the yield surface. φ is the dilation angle measured in the p-q plane at high confining pressure and this parameter was determined by sensitivity analysis. ϵ is a parameter, referred to as the eccentricity, that defines the rate at which the function approaches the asymptote.

3.1. Material models

The stress-strain curves obtained from compression tests for all adherence samples were utilized in the material model. For all samples, input values including yield and ultimate strengths, as well as the corresponding plastic deformation values under these strengths, were entered into the software tool. Elastic modulus values for each type of adherence sample were calculated separately and input into the software tool. For the adherence sample produced with Ordinary Portland Cement, the concrete strength was determined as 45 MPa. Within the scope of the concrete model, CDP model definitions were made. Fig. 8 illustrates the compressive behavior of the concrete [54].

In the ABAQUS, parameters entered for the compressive behavior of concrete include yield stresses and the corresponding inelastic unit strain values obtained based on these stresses. The inelastic behavior depicted in the graph refers to the portion following the stress and deformation values at yield. Inelastic strain values were obtained from Eq. 2 [55], and stress values were calculated according to Eq. 3.

$$\varepsilon_c^{in} = \varepsilon_c - \frac{\sigma_c}{E_0} \tag{2}$$

$$\sigma_c = (1 - d_c).E_0.(\varepsilon_c - \varepsilon_c^{pl}) \tag{3}$$

While the inelastic strain values were calculated and entered into the software, the program calculates the plastic strain values. Plastic strains were calculated from Eq. 4. In Eq. 5, d_c represents the damage parameter of concrete under compressive loading. The damage parameter represents the reduction in elastic stiffness due to loading after the maximum stress indicated in the graph shown in Fig. 7. The damage parameter holds significant importance for accurately portraying the plastic behavior of concrete within the software as close to reality. The damage parameter was calculated according to Eq. 5 [55].

$$\varepsilon_c^{pl} = \varepsilon_c^{in} - \frac{d_c}{(1 - d_c)} \frac{\sigma_c}{E_0} \tag{4}$$

$$d_c = 1 - \frac{\sigma_c/E_0}{\sigma_c/E_0 + \varepsilon_c^{in}(1 - b_c)} \tag{5}$$

The parameter b_c indicated in the equation represents the ratio of plastic strain to inelastic strain. Considering current studies, this value

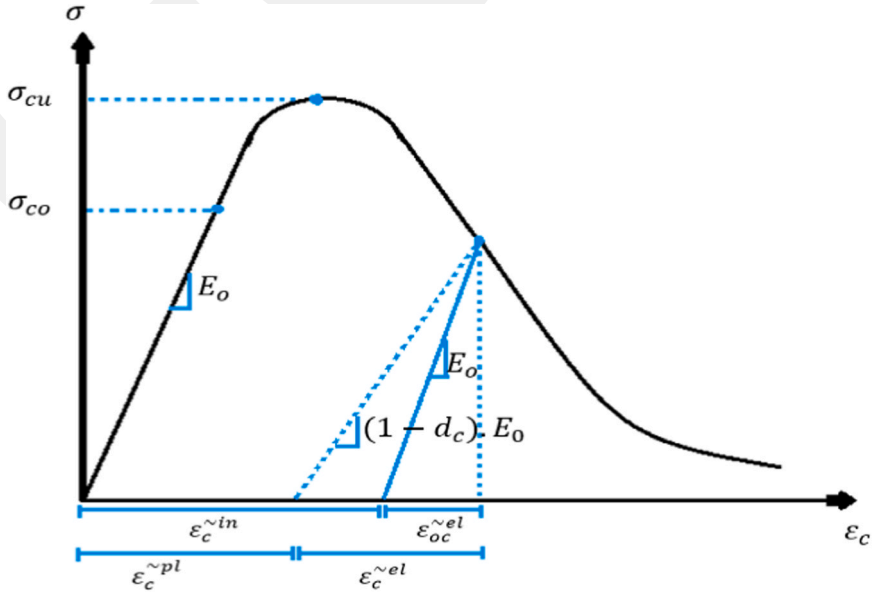

Fig. 8. Post-cracking compressive behavior of concrete.

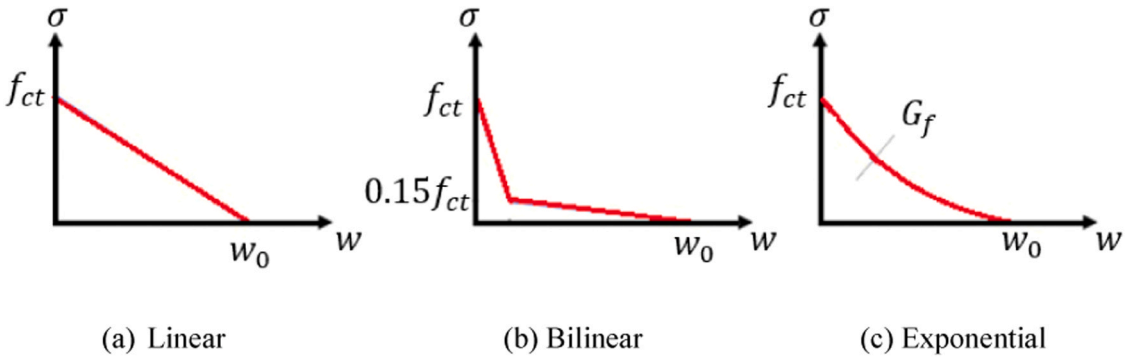

Fig. 9. Post-cracking tensile behavior of concrete.

for concrete was observed to fall within the range of 0.5 to 0.7 [56,57]. Linear, bilinear, and exponential models for concrete tensile stiffness are illustrated in Fig. 9 [58]. The term w in the graph represents crack width.

By entering all the relevant parameters related to concrete's compressive and tensile behavior, material properties for concrete were created. Compressive behavior graphs and damage parameters were derived by using data obtained from compression tests. Concrete compressive behavior graphs, which were plotted based on the results obtained from the cylinder samples produced with geopolymer concrete and the above formulas, are shown in Fig. 10. The stress-strain curve obtained from the experimental tensile tests of the rebar used in the study was also applied within the scope of the CDP model and presented as data to the program. The stress-plastic strain curve of the rebar entered into the program is shown below (Fig. 11). 200,000 MPa was entered as the rebar elasticity modulus and 0.3 was entered as the poisson value.

3.2. Interface constitutive model

The concept of cohesive behavior was employed to depict the deterioration of the bond between reinforced concrete elements. The existing traction-separation model assumes an initial phase of linear elasticity, which is then succeeded by the onset and progression of bond damage. The elastic behavior is mathematically expressed through an elastic constitutive matrix, establishing the relationship between nominal stresses and nominal strains along the interface [59].

The vector of nominal traction stresses comprises three elements: t_n, t_s, and t_t. These components represent the normal traction and the two shear tractions, respectively. The associated separations are represented by δ_n, δ_s, δ_t in Eq. 6 where the elastic behavior defined.

$$\begin{Bmatrix} t_n \\ t_s \\ t_t \end{Bmatrix} = \begin{bmatrix} K_{nn} & K_{ns} & K_{nt} \\ K_{ns} & K_{ss} & K_{st} \\ K_{nt} & K_{st} & K_{tt} \end{bmatrix} \begin{Bmatrix} \delta_n \\ \delta_s \\ \delta_t \end{Bmatrix} \tag{6}$$

By utilizing bond damage modeling, it becomes possible to replicate the progressive deterioration and eventual failure of the bond between a concrete body and steel reinforcement. This failure mechanism is composed of two fundamental elements: a criterion that determines when damage begins to occur, and a law that governs the subsequent progression of that damage.

The initiation of bond damage refers to the initial degradation of the cohesive response at a specific contact point. The degradation process is triggered when the contact stresses and/or contact separations meet specific criteria for damage initiation.

One commonly used criterion is the maximum stress criterion, where bond damage is assumed to commence when the ratio of maximum contact stress in Eq. 7 reaches a value of one. This criterion can be mathematically represented in Eq. 7.

$$\max\left\{\frac{\langle t_n\rangle}{t_n^0}, \frac{t_s}{t_s^0}, \frac{t_t}{t_t^0}\right\} = 1. \tag{7}$$

Maximum separation criterion: the bond damage is assumed to initiate when the maximum separation ratio in Eq. 8 reaches a value of one:

$$\max\left\{\frac{\langle \delta_n\rangle}{\delta_n^0}, \frac{\delta_s}{\delta_s^0}, \frac{\delta_t}{\delta_t^0}\right\} = 1 \tag{8}$$

The evolution law of bond damage explains how the cohesive stiffness progressively deteriorates once the initiation criterion is met. A scalar variable known as bond damage (D_b) represents the overall level of damage at the contact point. Initially, D_b is assigned a value of 0. In cases where damage evolution is considered, D_b gradually increases from 0 to 1 as the loading continues after the initiation of damage. The contact stress components are influenced by the damage based on Eq. 9.

$$t_n = \begin{cases} (1-D_b)\bar{t}_n, t_n > 0 \\ \bar{t}_n, t_n \le 0 \end{cases} \quad t_s = (1-D_b)\bar{t}_t, \tag{9}$$

The contact stress components, t_n, t_s, and t_t, are the calculated values based on the elastic traction-separation behavior, considering the current separations without any damage. In order to explain the progression of bond damage when a combination of normal and shear separations occurs across the interface, it proves beneficial to introduce an effective separation [60]. This effective separation is defined in Eq. 10.

$$\delta_m = \sqrt{\langle \delta_n\rangle^2 + \delta_s^2 + \delta_t^2}. \tag{10}$$

An evolution of the bond damage variable D_b given in Eq. 11 was used for exponential softening, that reduces in the case of damage evolution under a constant mode mix, temperature, and field variables.

$$D_b = 1 - \left\{\frac{\delta_m^0}{\delta_m^{\max}}\right\}\left\{1 - \frac{1-\exp\left(-a\left(\frac{\delta_m^{\max}-\delta_m^0}{\delta_m^f-\delta_m^0}\right)\right)}{1-\exp(-a)}\right\}. \tag{11}$$

In the expression above a is a non-dimensional parameter that defines the rate of damage evolution. The material and connection parameters used in the finite elements were calculated for each geopolymer concrete sample and OPC sample, and modeling was created using these values [61].

Contact was defined in order to model the interaction between concrete and reinforcement. The coefficient of friction between them was defined and entered into the program as 0.35. In addition, a hard contact definition was made under the name of the normal behavior tab. Also, the cohesive behavior between rebar and concrete was modeled. In this context, the cohesive behavior parameters as Knn, Kss and Ktt, which were also mentioned in the relevant study, were entered into the program. Knn (Normal Stiffness): This parameter represents the normal

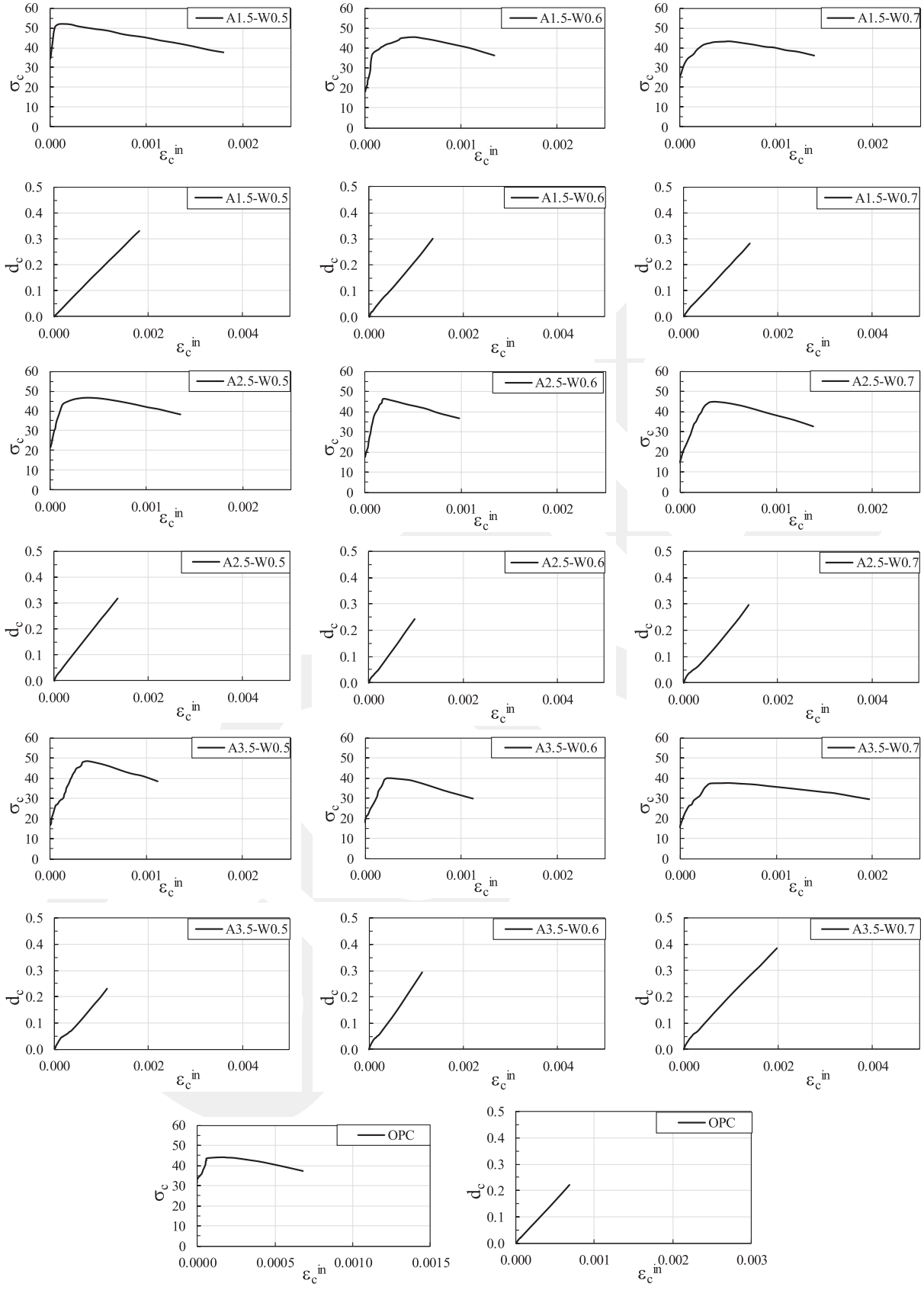

Fig. 10. Compressive-damage behavior graphs of adherence samples in numerical model.

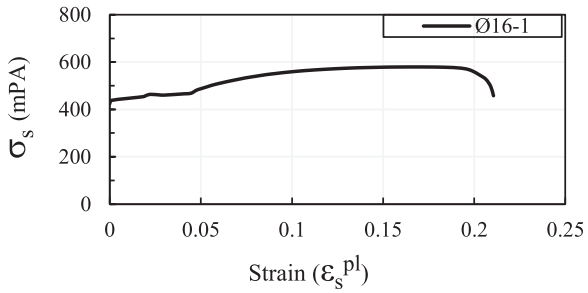

Fig. 11. Rebar stress-plastic strain curve.

(vertical) stiffness of the cohesive element interface. Normal stiffness is crucial for tensile loads in cohesive interactions between two materials. Kss (Shear Stiffness): It determines the shear stiffness on the cohesive element interface. Shear stiffness is important for lateral (parallel) shearing forces in cohesive interactions between two materials. Ktt (Tangential Stiffness): This parameter represents the tangential stiffness on the cohesive element's interface. In the damage section, nominal only and shear only values were given to the program separately. Contact and interaction elements were defined in the program by entering other parameters required for tangential behavior. As explained in detail in the above articles, modeling was completed by creating the analysis type and relevant boundary conditions. Analysis was carried out by plotting graphics as an output and other data presented in the study.

3.3. Meshing

For meshing, a finer and denser mesh size was selected in the area where the reinforcement would be located, while in other parts, the mesh size was increased. The simulation models were developed based on a 3D modeling tool, where deformable reduced-integration eight-node hexahedral elements (C3D8R) were selected. Various mesh sizes were employed in the analysis for both rebar and concrete. Following the analyses, a mesh size of 3.5 × 3.5 mm was determined for the rebar, while the lower portion, from which the concrete was removed in the specimen, was assigned a mesh size of 2.5 × 3 mm. This mesh size was selected to be thinner than the concrete in the upper section. Additionally, the mesh size for the upper concrete section, where there is no contact with the rebar during the stripping process, was designated as 3 × 10 mm.

The model was constructed with two components. Due to the symmetry of the specimen, only half of the specimen was modeled. The portion not included in the bond length with the help of a plastic pipe in the experimental section was simulated in the numerical model by forming a void with the diameter and length of the plastic pipe. In the experimental study, the 80 mm long region where adherence will occur between the rebar and the concrete, and the 120 mm long region covered with a plastic sheath and where the rebar does not interact with the concrete in the experimental study, were modeled by creating a separate opening. In this way, the bond length during the analysis was the same as the length formed in the experimental samples. Model, support and mesh views are shown in Fig. 12.

3.3.1. Mesh sensitivity

The finite element analysis of the A1.5W0.5 sample of the geopolymer concrete series were considered as an example within the scope of the mesh sensitivity section. Analyses were made by changing the mesh sizes of the relevant sample as fine, medium and coarse. The mesh sizes of the relevant samples are presented in the Table 5. Various mesh sizes were employed in the analysis for both rebar and concrete.

When bond stress-slip curves are compared, decreasing the mesh size causes a relative decrease in the bond stress value. The mesh size that is most compatible with the experimental data of the A1.5W0.5 sample. Following the analyses, a mesh size of 3.5 × 3.5 mm was determined for the rebar, while the lower portion, from which the concrete was removed in the specimen, was assigned a mesh size of 2.5 × 3 mm. This mesh size was selected to be thinner than the concrete in the upper section. Additionally, the mesh size for the upper concrete section, where there is no contact with the rebar during the stripping process, was designated as 3 × 10 mm.

3.4. Boundary conditions

In the numerical modeling, the modeling was carried out to correspond appropriately to the specimen properties produced in the experimental section. The objective was to ensure that the geometric properties and boundary conditions represented the experimental setup

Table 5
Mesh sizes of samples.

Sample Name	Rebar Mesh Size (mmxmm)	Concrete Bottom (mmxmm)	Concrete Top (mmxmm)
A1.5W0.5	3.5 × 3.5	3.75 × 4.5	4.5 × 10
A1.5W0.5-1	2.5 × 2.5	2.5 × 3	3 × 10
A1.5W0.5-2	1.75 × 1.75	2.25 × 2.5	2.25 × 10
A1.5W0.5-3	7 × 7	2.5 × 9	9 × 10
A1.5W0.5-4	10 × 10	4.5 × 5	4.5 × 10
A1.5W0.5-5	15 × 15	8 × 18	10 × 18

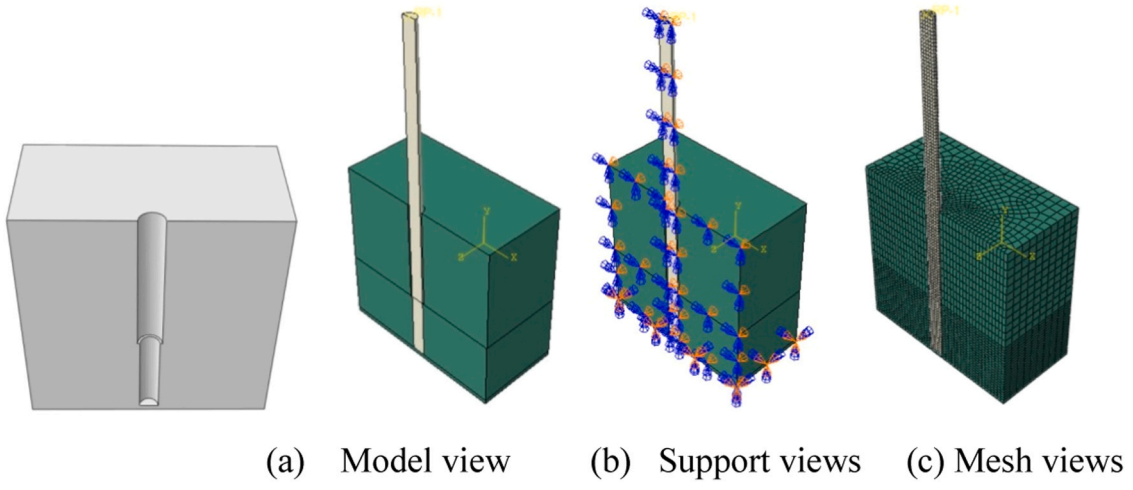

Fig. 12. The schematic views of modeling details.

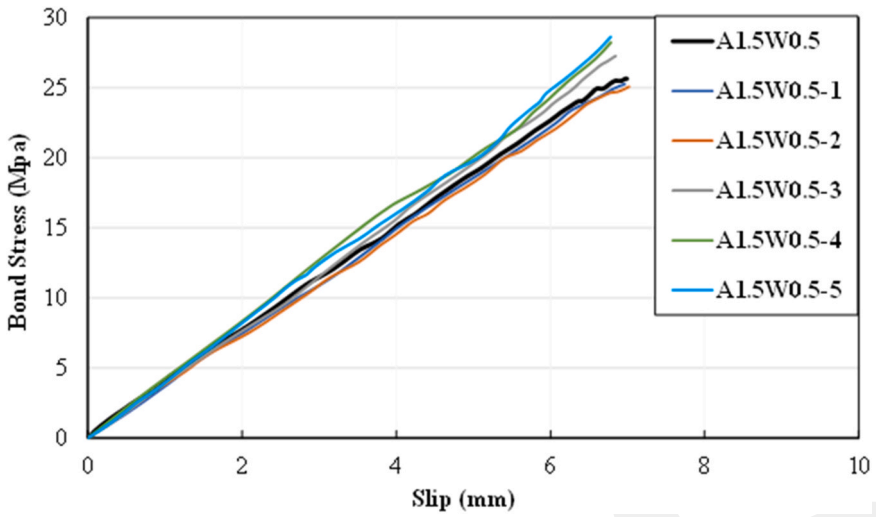

Fig. 13. Bond stress-slip curves of analyses of sample geopolymer concrete at different mesh sizes.

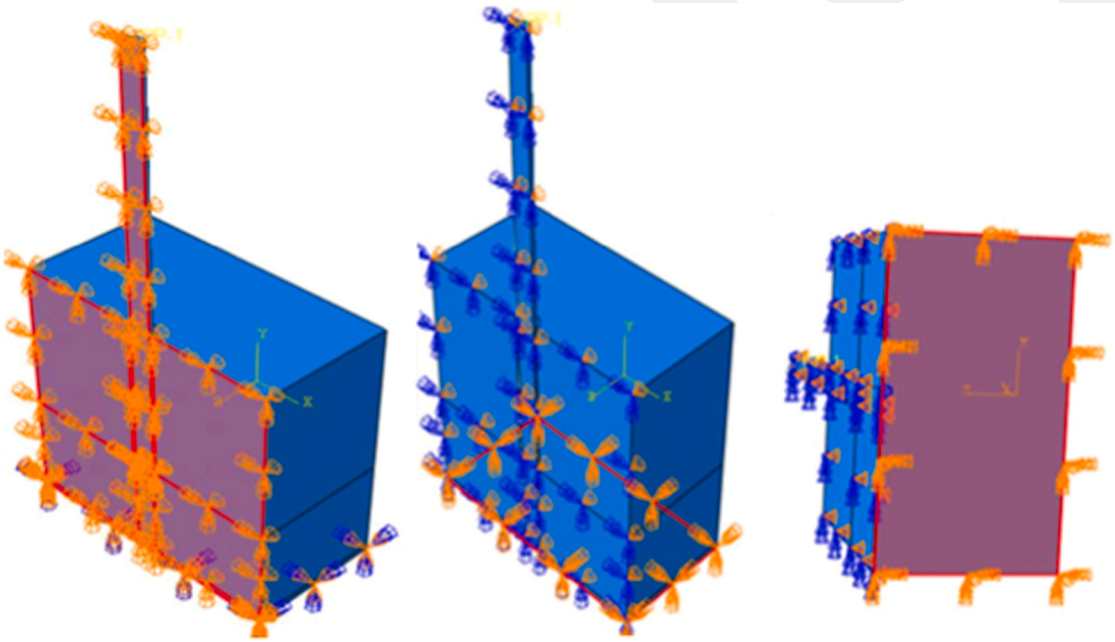

Fig. 14. Side and bottom surface boundary condition.

accurately. Boundary conditions in the finite element sample were arranged in two ways. In order to clearly observe the analyses and behaviors, half of the sample was modeled symmetrically. In this context, as a boundary condition, the side surface on which half of the reinforcement modeled were constrained against displacement along the z axis and prevented from undergoing rotation in the x and y directions (Fig. 14). The lower part of the sample was modeled as a fixed support in order to be similar to the mechanism used in experimental studies. Displacements and rotations in the X, Y and Z directions were prevented. (Fig. 14).

3.5. Loading and analysis method

A vertical displacement was defined at the upper part of the reinforcement as the loading method. Structural reactions and behavior of the adherence samples were analyzed under the relevant displacement demand, and the load values were measured from the support points under loading depending on the displacement, and bond stress-slip curves were obtained in line with these values. Since the displacement definition was made, no data regarding the loading rate was entered. During the loading phase, amplitude was defined and the analysis was divided into steps. Dynamic/Explicit was used as the analysis method. Dynamic Explicit was applied as the analysis type and the time period was entered as 0.1 s. During the loading, the analysis was continued step by step until the target displacement was reached in relation to the target analysis time.

The Dynamic/Explicit method is generally used in cases where the sample reaches the collapse mechanism. Since damping and inertia effects of the material were included in the analysis in explicit methods, it was determined that it was more appropriate to be used within the scope of this study.

Table 6
Failure modes of GPC and OPC pull-out test specimens.

Sample ID	Sample Number		
	1	2	3
A1.5W0.5	P	P	P
A1.5W0.6	P	S-B	P
A1.5W0.7	P	P	P
A2.5W0.5	S	S	S
A2.5W0.6	S	S	S
A2.5W0.7	S-B	S	S
A3.5W0.5	S	S	S
A3.5W0.6	S	S	S
A3.5W0.7	S	S	S
OPC	P	P	P

Note: S, P and S-B denote splitting, pull out and splitting-bond failure respectively.

4. Results and discussion

4.1. Experimental results

In this section, the results obtained from the test were thoroughly investigated in terms of failure mode, mechanical characteristics, bond stress behavior, the effect of SS/SH ratio and AA/FA ratio on the bond strength of the GPC, and a comparison of experimental tests with previous studies.

4.1.1. Failure modes

The fracture modes of the test specimens are discussed in this section. At the end of the experiment, upon investigating all specimens, it was observed that the samples exhibited damage in the forms of typical splitting failure, splitting-bond failure, or pull-out failure. It was observed that the samples in the form of typical splitting failure, splitting-bond failure or pull-out failure were damaged by investigating all the samples at the end of the tests. Typical rupture damage type is the type of damage that occurs when radial cracks occur from the surface of the reinforcement and these cracks progress rapidly in the longitudinal direction and the geopolymer concrete suddenly fractures without too much shear in the rebar [13]. In pull out damage, the geopolymer is characterized by the interface between the concrete and the reinforcement, a significant slip occurs in the reinforcement, but no splitting damage is observed in the concrete. If the sample is damaged by both the debonding of the reinforcement and the formation of splitting damages in the concrete, this is called splitting-pull out damage. The fracture modes of each sample are given in Table 6.

There are images of the fracture modes in Fig. 15. Studies have shown that the parameters that play an active role in the damage type are the fly ash content of the mixture and the concentration of the alkali activator [62]. The factors affecting the bond strength in terms of experimental behavior are the quality of the geopolymer such as gel compositions and strength, the bar length of the reinforcement, the embedded length of the reinforcement, and the thickness of the reinforcement concrete cover [27]. Specimens with short anchorage length reach their capacities due to debonding of the reinforcement, while specimens with longer embedment lengths reach their capacities

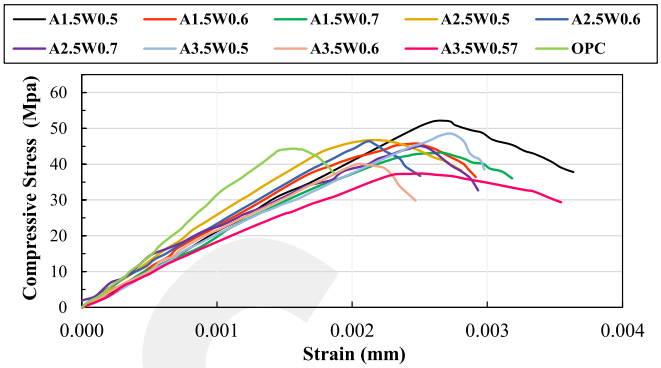

Fig. 16. Compressive stress-strain curves of GPC and OPC samples.

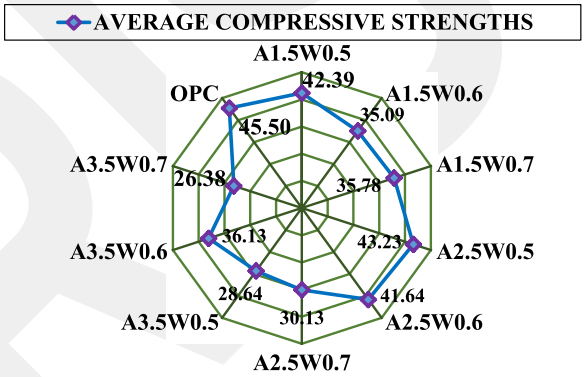

Fig. 17. Average compressive strength values of OPC and GPC samples.

Table 7
Modulus of elasticity values of adherence samples.

Sample ID	E (MPa)
A1.5W0.5	20,618
A1.5W0.6	23,220
A1.5W0.7	20,203
A2.5W0.5	26,389
A2.5W0.6	24,105
A2.5W0.7	19,918
A3.5W0.5	20,731
A3.5W0.6	22,075
A3.5W0.7	18,617
OPC	21,021

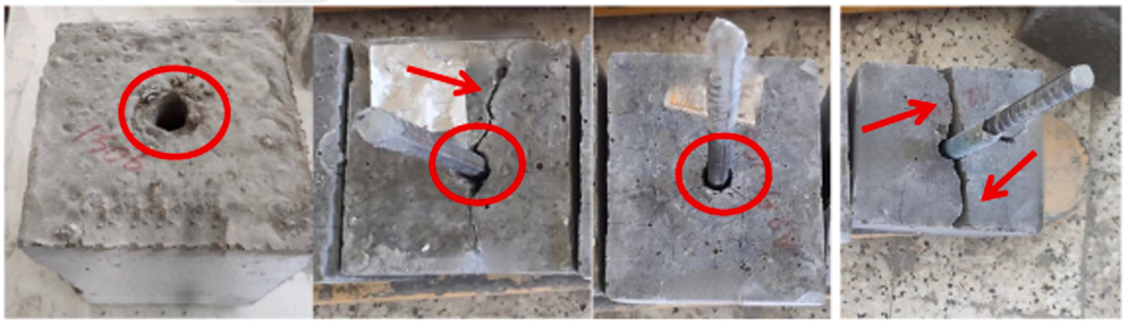

Fig. 15. Failure patterns after pull-out test.

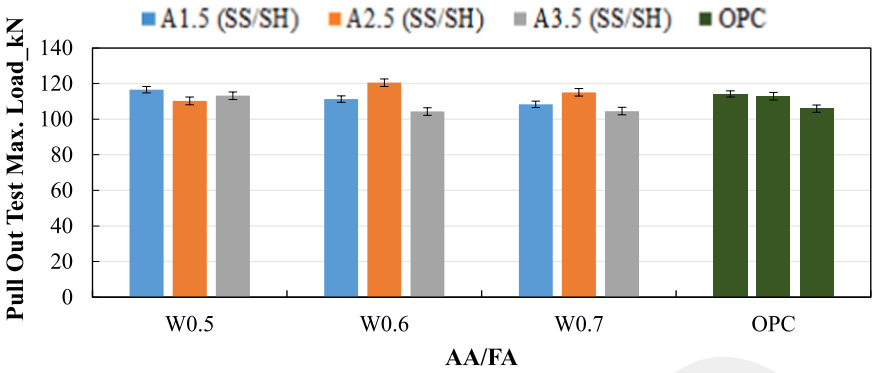

Fig. 18. Maximum bond load values.

Table 8
Experimental results of adherence samples.

Specimen Designation	Peak Load Fmax (kN)	Bond Strength τ (MPa)	Standard Deviation for Bond Strenght	Slip at Peak Load (mm)	Normalized Bond Strength $k = \frac{\tau}{\sqrt{f_c}}$	$\frac{k}{k_{cc}}$
OPC-2	112.6	28		16	4.2	1
OPC-3	105.8	26.3		15	3.9	0.93
A1.5W0.5-1	118.3	29.4	0.35	20.8	4.5	1.08
A1.5W0.5-2	115.4	28.7		17.8	4.4	1.05
A1.5W0.5-3	116.6	29		22.5	4.5	1.06
A1.5W0.6-1	116.9	29.1	1.18	25.9	4.9	1.17
A1.5W0.6-2	109	27.1		13.7	4.6	1.09
A1.5W0.6-3	108.7	27		18.8	4.6	1.09
A1.5W0.7-1	114.6	28.5	2.34	16.3	4.8	1.13
A1.5W0.7-2	97.7	24.3		10	4.1	0.97
A1.5W0.7-3	113.4	28.2		19.9	4.7	1.12
A2.5W0.5-1	105.8	26.3	1.22	9.4	4	0.95
A2.5W0.5-2	115.4	28.7		20.2	4.4	1.04
A2.5W0.5-3	112.2	27.9		17.3	4.2	1.01
A2.5W0.6-1	117.4	29.2	0.70	16.7	4.5	1.08
A2.5W0.6-2	121.8	30.3		27.2	4.7	1.12
A2.5W0.6-3	122.6	30.5		27.7	4.7	1.13
A2.5W0.7-1	109.4	27.2	1.72	17.2	5	1.18
A2.5W0.7-2	122.6	30.5		28.2	5.6	1.32
A2.5W0.7-3	112.6	28		20.3	5.1	1.21
A3.5W0.5-1	109.4	27.2	1.01	21.2	5.1	1.21
A3.5W0.5-2	112.6	28		19.4	5.2	1.25
A3.5W0.5-3	117.4	29.2		26.5	5.5	1.3
A3.5W0.6-1	100.5	25	1.08	9	4.2	0.99
A3.5W0.6-2	109	27.1		15.8	4.5	1.07
A3.5W0.6-3	102.9	25.6		16.2	4.3	1.01
A3.5W0.7-1	105	26.1	0.78	23.7	5.1	1.21
A3.5W0.7-2	105.4	26.2		20.4	5.1	1.21
A3.5W0.7-3	99.7	24.8		6.9	4.8	1.15

*k_{cc} is the value of k for OPC specimens.

due to the splitting damage of geopolymer concrete [63]. As the quality of the geopolymer increases, the reinforcement is pulled out after exceeding the peak bond load value [24]. Since the increase in the SS/SH ratio changed the geopolymer concrete quality, it was observed from the tests that the concrete splits without exhibiting reinforcement debonding behavior. This failure mode occurs when the reinforcement comes out of the concrete without fracturing the reinforcement or even cracking the concrete. Since the increase in the SS/SH ratio changes the geopolymer quality, it has been observed in the experiments that the concrete splits without showing the reinforcement stripping behavior with the increase in this ratio. This failure mode occurs when the reinforcement comes out of the concrete without breaking the reinforcement or even cracking the concrete. This situation occurs when the radial forces applied by the loaded bar are less than what the surrounding concrete can resist, but there are higher tangential forces than the concrete's strength can withstand. With sufficient embedment length and prevention of debonding, the reinforcement can reach yield strength and transition to a pullout failure mode before experiencing bond failure. The literature encounters cases of direct pullout of the reinforcement [64]. It was concluded that the bond between the GPC concrete and the reinforcement and the lateral strength were stronger with the increase of the SS/SH ratio. In the series where the SS/SH ratio was 2.5 and 3.5, the reason for the concrete to split and reach the collapse mode was that the displacement value reached the failure mode by debonding the reinforcement, compared to the samples with a SS/SH ratio of 1.5.

4.1.2. Mechanical characteristics

This section presents the results of compressive strength tests

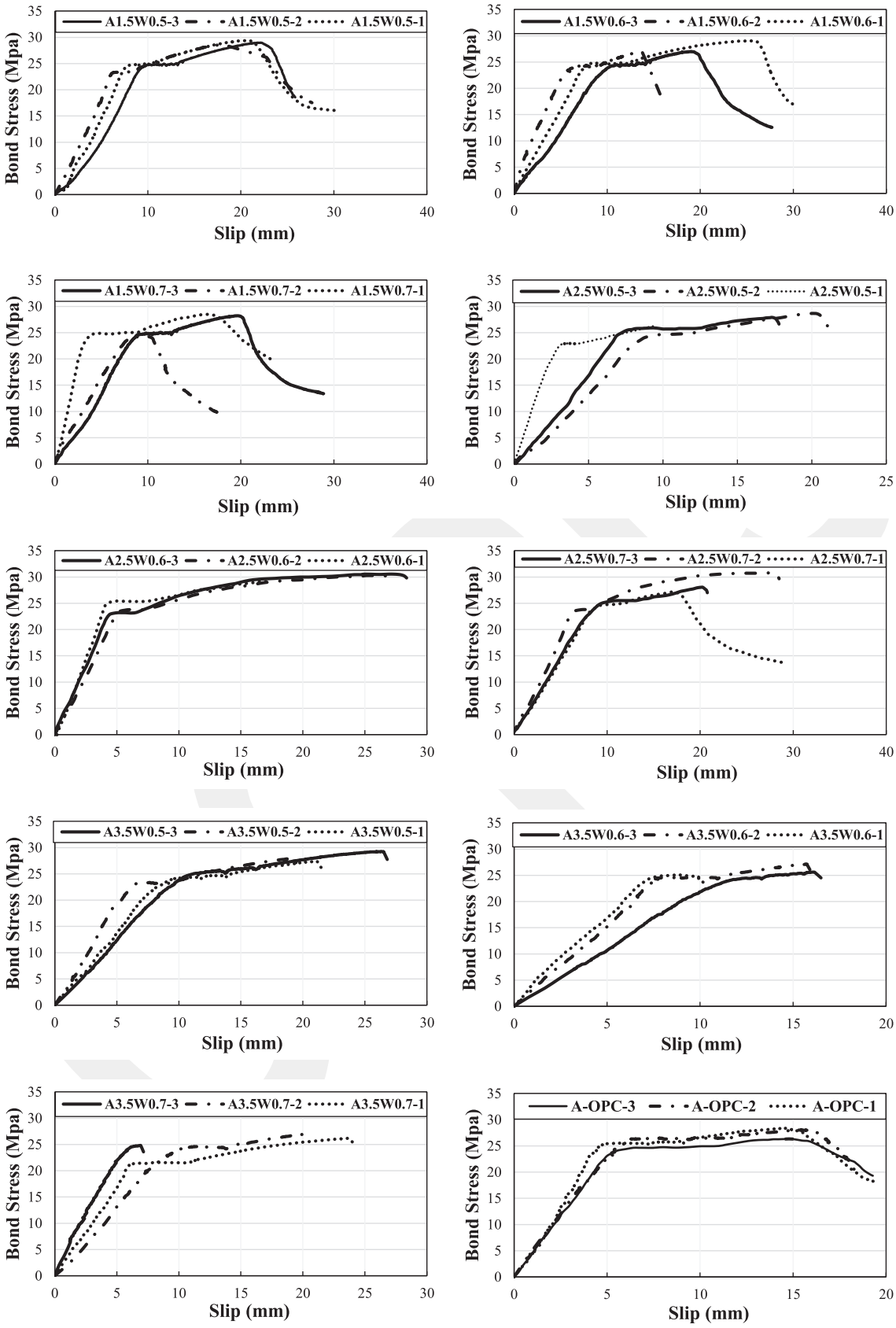

Fig. 19. The bond stress-slip curves obtained from experiments.

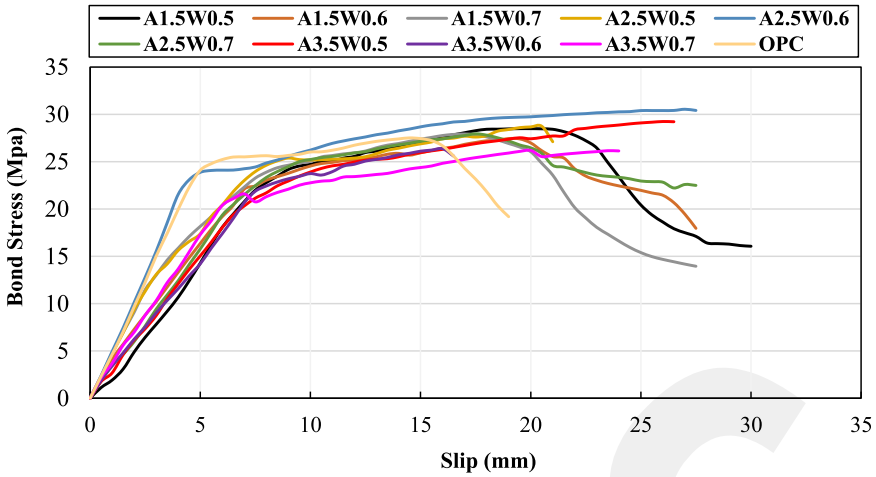

Fig. 20. The bond stress-slip curves obtained from experiments.

Table 9
Comparison between previous researches and experimental results.

Specimen	d_b (mm)	c (mm)	c/d_b	l_d (mm)	d_b/l_d	τ (Experimental) (MPa)	τ (Kim and Park[65]) (MPa)	τ (Orangun[66]) (MPa)
OPC-1	16	92	5.75	80	0.2	28.4	26.48	30.90
OPC-2	16	92	5.75	80	0.2	28.1	27.44	32.02
OPC-3	16	92	5.75	80	0.2	26.3	28.02	32.69
A1.5W0.5-1	16	92	5.75	80	0.2	29.4	26.60	31.00
A1.5W0.5-2	16	92	5.75	80	0.2	28.7	26.37	30.73
A1.5W0.5-3	16	92	5.75	80	0.2	29.0	26.14	30.46
A1.5W0.6-1	16	92	5.75	80	0.2	29.1	25.25	29.43
A1.5W0.6-2	16	92	5.75	80	0.2	27.1	22.66	26.41
A1.5W0.6-3	16	92	5.75	80	0.2	27	23.99	27.96
A1.5W0.7-1	16	92	5.75	80	0.2	28.5	23.87	27.82
A1.5W0.7-2	16	92	5.75	80	0.2	24.3	24.28	28.30
A1.5W0.7-3	16	92	5.75	80	0.2	28.2	24.52	28.57
A2.5W0.5-1	16	92	5.75	80	0.2	26.3	26.63	31.03
A2.5W0.5-2	16	92	5.75	80	0.2	28.7	27.02	23.76
A2.5W0.5-3	16	92	5.75	80	0.2	27.9	26.23	19.98
A2.5W0.6-1	16	92	5.75	80	0.2	29.2	26.13	31.03
A2.5W0.6-2	16	92	5.75	80	0.2	30.3	25.29	31.49
A2.5W0.6-3	16	92	5.75	80	0.2	30.6	26.95	30.57
A2.5W0.7-1	16	92	5.75	80	0.2	27.2	22.23	25.91
A2.5W0.7-2	16	92	5.75	80	0.2	30.8	20.35	23.72
A2.5W0.7-3	16	92	5.75	80	0.2	28	23.96	27.92
A3.5W0.5-1	16	92	5.75	80	0.2	27.4	22.46	26.17
A3.5W0.5-2	16	92	5.75	80	0.2	28	20.86	24.31
A3.5W0.5-3	16	92	5.75	80	0.2	29.3	21.66	25.24
A3.5W0.6-1	16	92	5.75	80	0.2	25.1	24.33	28.36
A3.5W0.6-2	16	92	5.75	80	0.2	27.1	21.90	25.53
A3.5W0.6-3	16	92	5.75	80	0.2	25.6	26.56	30.95
A3.5W0.7-1	16	92	5.75	80	0.2	26.2	19.34	22.54
A3.5W0.7-2	16	92	5.75	80	0.2	27	24.78	28.88
A3.5W0.7-3	16	92	5.75	80	0.2	24.8	17.61	20.52

conducted on 3 cube specimens produced for each mixture ratio. Compressive stress strain curves of all GPC and OPC samples obtained from compression tests are presented in Fig. 16. The average compressive stress values obtained from the compression tests are illustrated in Fig. 17. All measurements were performed 28 days after casting. Three samples were tested for each SS/SH ratio and AA/FA ratio, and the results were averaged. The average compressive strength values were 42.39, 35.09, 35.78 MPa for A1.5W0.5, A1.5W0.6, A1.5W0.7 samples respectively with SS/SH ratios of 1.5 while, the average strengths were 43.23, 41.64, 30.13 MPa for A2.5W0.5, A2.5W0.6, A2.5W0.7 respectively with SS/SH ratios of 2.5, and the average strengths were calculated as 28.64, 36.13, 26.38 MPa for A3.5W0.5, A3.5W0.6, A3.5W0.7, respectively with SS/SH ratios of 3.5. The average compressive strength of reference OPC samples produced to compare the results was calculated as 45.50 MPa.

In conclusion, the average compressive strength values of specimens with SS/SH ratios of 1.5 and 2.5 were similar values, while a relatively lower value was recorded for the 3.5 series. The highest average compressive strength belonged to the OPC as 45.5 MPa. The compressive strength had no significant change in specimens with AA/FA ratios of 0.5 and 0.6, whereas a decrease in compressive strength was observed in specimens with a ratio of 0.7. The highest average compressive strength belongs to the A2.5W0.5 series for the adherence specimens. In addition, the elastic modulus values of the samples given in Table 7 were calculated by using the stress-strain curves obtained from the cylindrical sample compressive tests.

By investigating the elasticity modules, the series with the highest elasticity modulus value was the A2.5W0.5 series, as in the compressive strengths. Similar to the compressive strengths, no decrease was observed in the series with AA/FA ratio of 0.5 and 0.6, while a relative

Table 10
Comparison of experimental and numerical yield and slip results.

Samples	Experimental Results		Experimental Average Results		Numerical Results	
	Yield Stress MPa	Slip mm	Yield Stress MPa	Slip mm	Yield Stress MPa	Slip mm
A1.5W0.5-1	24.8	8.65	24.3	8.61	25.51	6.92
A1.5W0.5-2	23.4	6.67				
A1.5W0.5-3	24.7	10.50				
A1.5W0.6-1	24.7	8.61	24.4	8.79	28.19	7.07
A1.5W0.6-2	24.2	6.54				
A1.5W0.6-3	24.4	11.22				
A1.5W0.7-1	24.8	4.20	24.5	7.61	23.48	6.83
A1.5W0.7-2	24.1	8.64				
A1.5W0.7-3	24.7	9.99				
A2.5W0.5-1	22.9	3.38			30.56	6.95
A2.5W0.5-2	24.6	9.92	24.4	7.1		
A2.5W0.5-3	25.8	8.10				
A2.5W0.6-1	25.4	4.89	24.1	5.4	28.29	6.72
A2.5W0.6-2	23.8	5.92				
A2.5W0.6-3	23.2	5.38				
A2.5W0.7-1	24.7	9.75	24.6	8.9	23.33	6.61
A2.5W0.7-2	23.8	7.12				
A2.5W0.7-3	25.2	9.73				
A3.5W0.5-1	24.1	9.92	24.2	9.6	24.47	6.81
A3.5W0.5-2	23.3	7.16				
A3.5W0.5-3	25.1	11.57				
A3.5W0.6-1	24.7	7.49	24.6	9.3	23.06	6.62
A3.5W0.6-2	24.6	8.23				
A3.5W0.6-3	24.4	12.23				
A3.5W0.7-1	21.4	6.53	23.5	9.9	19.46	6.67
A3.5W0.7-2	24.4	16.65				
A3.5W0.7-3	24.7	6.42				
OPC-1	25.5	5.53	25.5	6.2	24.26	6.73
OPC-2	26.3	6.53				
OPC-3	24.7	6.41				

decrease was observed in the series with 0.7. Increasing the SS/SH ratio from 1.5 to 2.5 had a positive effect on compressive strength and elastic modulus, while in the series where it is 3.5, it led to a decrease in these values.

4.1.3. Bond stress behaviour

This section presents the results of the pull-out test. Firstly, the bond load obtained from the test results are presented in Fig. 18.

The pull-out test results of all GPC mixtures, along with the reference OPC, are summarized in Table 8. The results encompass fracture mode, peak load, corresponding average bond stress, and slip. The bond stress between the concrete matrices and the reinforcement was assumed to be uniformly distributed along the embedment length of the rebar.

When the standard deviations were investigated, it was figured out that the experimental results were within the range.

The bond stress-slip graphs obtained from the pull-out tests are presented in Fig. 19. In general, the series exhibited behavior close to their respective averages, and the curves within a series are in good agreement with each other. The highest load value of 122.89 kN was observed in the A2.5W0.6 series in the bond tests. The highest average load value also belonged to the A2.5W0.6 series, which is 120.5 kN. When evaluating the results obtained from the bond tests of OPC and GPC based specimens, it was observed that the highest bond strength values for OPC based specimens were lower than those of GPC based specimens, except for the A3.5W0.6 and A3.5W0.7 samples. By investigating debonding values, the maximum debonding value obtained from the OPC samples was lower than the debonding value of the GPC samples. When the k/k_{cc} ratios determined for the comparison of the adherence performances of the GPC and OPC samples and the k/k_{cc} ratios where OPC concrete was considered as the reference, it was observed that geopolymer concrete provides values above 1.00 in almost all series compared to OPC concrete. This indicates that geopolymer concrete has a more positive effect on bond performance.

The average bond stress-slip curves obtained from three samples of each different sample type are shown in Fig. 20. Within the scope of the study, all series were compared within themselves.

As seen from the bond stress-slip graphs, the rebar slips due to the lower ratio, resulting in a demand for displacement in the series where the SS/SH ratio is 1.5. Furthermore, a similar observation was made that after reaching the maximum load, the reinforcement continued to slip without a sudden drop in the OPC series. The experiments terminated for the series with SS/SH ratios of 2.5 and 3.5 due to concrete splitting after reaching the maximum load. Both in terms of failure mode and bond stress-slip curves, a similar behavior was observed between OPC and GPC for the series with an SS/SH ratio of 1.5.

4.1.3.1. Effect of SS/SH ratio and AA/FA ratio on the bond strength of the GPC. In GPC specimen mixtures, increasing the Na_2SiO_3/NaOH ratio from 1.5 to 2.5 enhances the bond strength [27]. Accordingly, the highest compressive strength and bond load were obtained from specimens with an SS/SH ratio of 2.5, while the highest maximum displacement value was obtained from specimens with a ratio of 1.5. Considering the AA/FA ratios, the highest compressive strength and maximum displacement were recorded for the samples with 0.5 ratio, while the highest value in terms of bond load and bond stress value belonged to the samples with the AA/FA ratio of 0.6. For the SS/SH ratio, compressive strength and bond load were obtained from specimens with parallel ratios. In terms of AA/FA, this parallelism holds true for compressive strength and maximum displacement. As seen from Table 4, samples with SS/SH ratio of 3.5 exhibited the worst performance in terms of compressive strength, bond load, and maximum displacement, while samples with a ratio of 0.7 for AA/FA ratio exhibited the lowest performance. According to this, an increase in the SS/SH ratio improves mechanical properties such as compressive strength and bond load, whereas an increase in the AA/FA ratio, especially in the series with a ratio of 0.7, leads to the opposite effect. The reason for this is that an increase in the sodium silicate content up to a certain level enhances mechanical properties due to increased reactivity of fly ash and increased silicate particle distribution within the matrix, leading to enhanced polymerization. However, exceeding a certain amount hinders the formation of geopolymers due to the inability of fly ash particles to react sufficiently with sodium hydroxide in the mixture, thereby negatively affecting mechanical properties. Again, due to its negative impact on geopolymers, an increase in the amount of NaOH based on the fly ash content adversely affects geopolymerization,

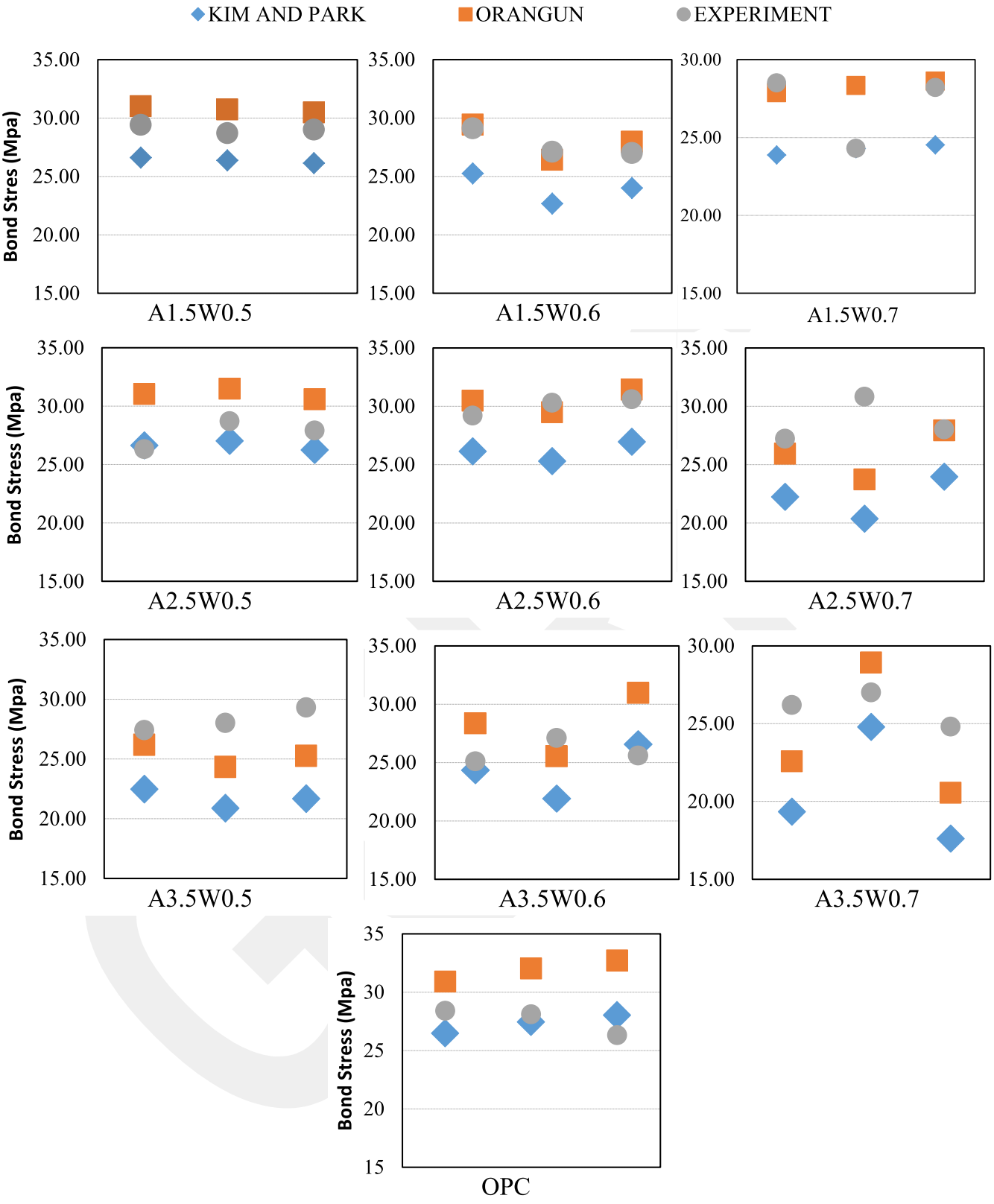

Fig. 21. Comparison of experimental data and results from previous studies.

leading to a decrease in mechanical properties.

4.1.4. Comparison of the experimental test with the previous studies

The bond stresses obtained from the tests were compared with the equations from previous studies. Kim and Park [65] proposed Eq. 12 [34] to predict bond stress for geopolymer concretes in their study.

$$\tau_u = \sqrt{f_c'}\left[2.07 + 0.2\left(\frac{c_{\min}}{d_b}\right) + 4.15\left(\frac{d_b}{l_d}\right)\right] \quad (12)$$

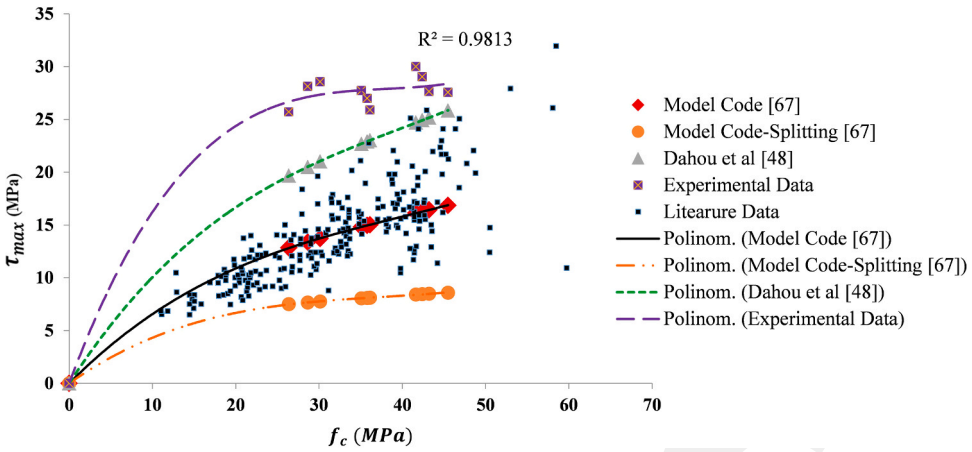

Fig. 22. Adherence Pressure - Compressive Strength Relationship with Experimental and Analytical Data.

where c_{min} represents the minimum concrete cover (mm), d_b is the diameter of the rebar (mm), l_d is the bond length (mm) and $f_c^{'}$ is the compressive strength obtained from geopolymer concrete specimens (MPa).

In another study, Orangun et al. [66] proposed a formula to determine the bond stress. This formula is given in Eq. 13. The results obtained from the equations and experimental results are presented in Table 9 and Fig. 21.

$$\tau_u = 0.083045\sqrt{f_c^{'}}\left[1.2+3\left(\frac{c}{d_b}\right)+50\left(\frac{d_b}{l_d}\right)\right] \quad (13)$$

As can be understood from Table 9 and Fig. 21, the experimental data of the specimens exhibited close results with the equation proposed by Orangun et al. [66] in six out of nine geopolymer series. In the case of OPC specimens, it was observed that the bond stress values obtained by using the formula proposed by Kim and Park [65] exhibit similarity. In a study, if c/d_b is limited to 4.0, it is proposed that the equation suggested by Orangun et al. [66] would be the most suitable equation for experimental data [21]. It was observed that the bond stress values calculated using the respective studies exhibit similar values to the experimental results for the series with AA/FA ratios of 0.5 and 0.6. However, a deviation in values was identified in the series with a ratio of 0.7.

4.1.5. Relationship bond to compressive strength with comparison of the experimental test with the previous theoretical studies

The relationship between bond strength and compressive strength were revealed. This relationship was compared with bond strength predictions and data in the literature. In the bond strength for OPC concrete is given [67]:

$$\tau_{b-OPC} = 2.5x\sqrt{f_c} \text{ for pull out failure} \quad (14)$$

$$\tau_{b-OPC} = 7.0x\left(\frac{f_c}{20}\right)^{0.25} \text{ for splitting failure} \quad (15)$$

fc, the average cylinder concrete compressive strength. According to the results obtained from 260 pull-out experimental studies, the following equation was created [48]:

$$\tau_{b-GPC} = 3.83x\sqrt{f_c} \quad (16)$$

In this study, the correlation coefficient was found to be 0.83 [35]. As seen, Eq. (16) is similar to Eq. (14) except for its constant coefficients. In the light of these equations, it is revealed that GPC gives 53% better adherence strength. In Fig. 22, the relationship between bond strength and compressive strength was discussed by comparing with analytical studies. When the curve of the experimental data was investigated, it was observed that the correlation coefficient was 0.98. When compared the experimental data with the data in the literature [10,68–71], it was figured out that the higher adherence strength results were obtained in this study.

The equation obtained within the scope of the study is;

$$\text{It was} \tau_{b-GPC} = 0.0005f_c^3 - 0.0548f_c^2 + 2.1231f_c \quad (17)$$

Also the mechanical properties of GPC are mainly influenced by not only the chemical characteristics of fly ash, alkali activators and binder ratios but also microstructure of geopolymer concrete. The existence of N-A-S-H gel in the microstructure of geopolymer concrete improves the mechanical properties with the increase in geopolymerization. Furthermore, N-A-S-H gel contributes to the strength of the interfacial transition zone (ITZ) between aggregate and geopolymer matrix by improving the aggregate interface and the GPC matrix. After all, ongoing geopolymerization process provides to more compact and denser matrix structure which results in higher mechanical properties such as compressive strength and bond strength since there is a proportion between both strengths. By increasing the compressive strength there is an increase in bond strength. Since the load transfer in structural members depends on the bond strength of concrete the higher bond strength is quite important for geopolymer concrete[72].

4.2. Numerical results

This section includes numerical results, and a comparison is made between the obtained analysis results and the experimental data.

4.2.1. Analytic failure and damage results

The results of finite element analyses carried out in the ABAQUS are presented in Figs. 23–26. When investigating the compressive damage distributions shown in Fig. 23, parallel results were obtained in comparison to stress-strain curves obtained from the compression tests. The most intense compressive damage distribution was observed in the OPC samples. In the series with an SS/SH ratio of 1.5, an increase in the AA/FA ratio reduced the compressive damage distribution, while in the series with a ratio of 3.5, an increase in the distribution was noted. The series with the least observed compressive damage was the A2.5 series, where the bond loads were calculated to be the highest. OPC specimens exhibited more ductile behavior than geopolymer specimens.

The finite element models' Scalar stiffness degradation (SDEG) views are presented in Fig. 24. SDEG stiffness degradation is a crucial aspect of simulating the behavior of structures under damage or collapse. In the context of finite element analysis, "scalar stiffness degradation" typically involves reducing the stiffness (elastic properties) of a material due to its exposure to damage, yielding, or other failure modes. This allows the simulation to capture the progressive degradation of the specimen as the analysis progresses. This modeling alters the material's elastic

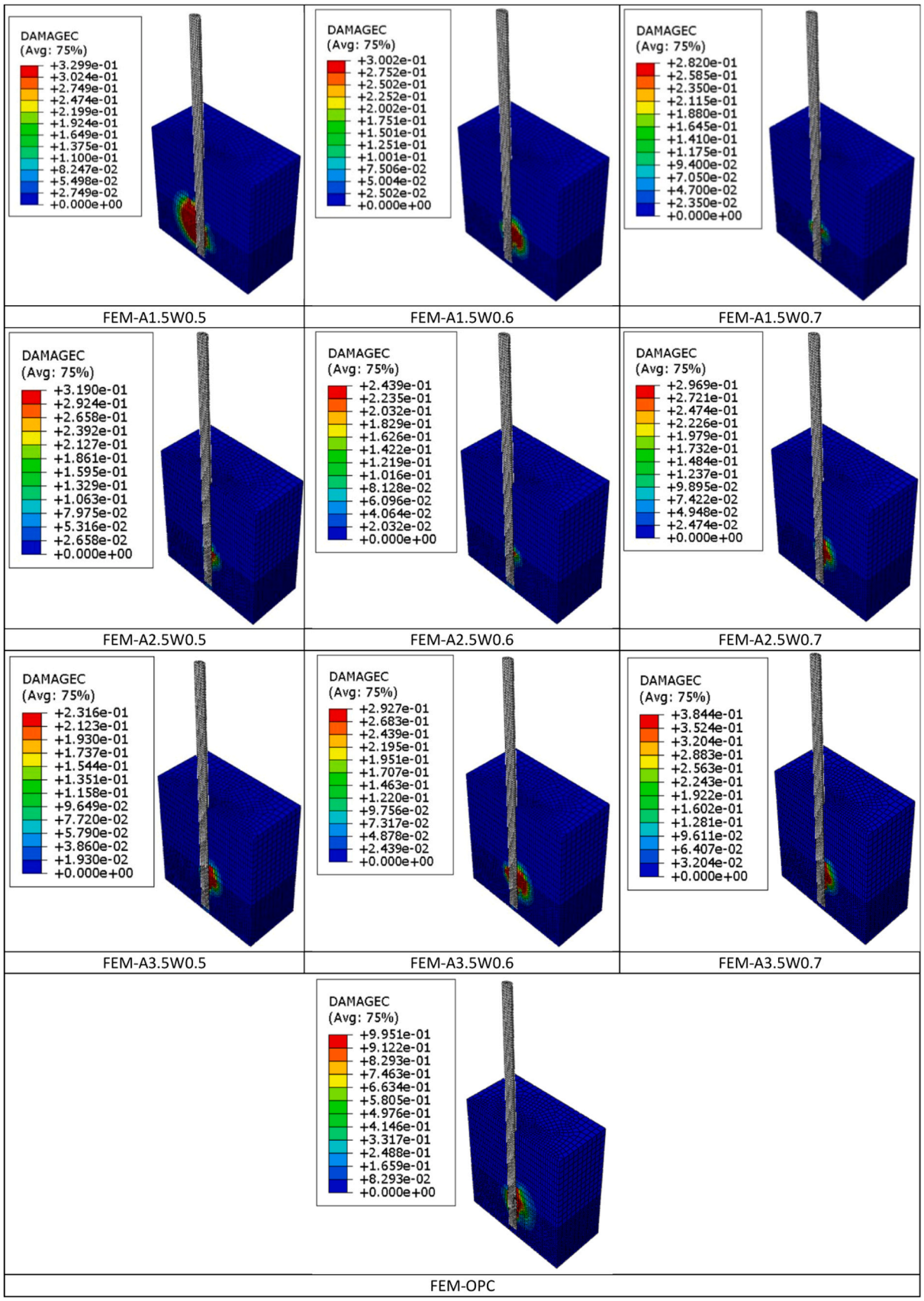

Fig. 23. Compressive damage distribution of finite element models.

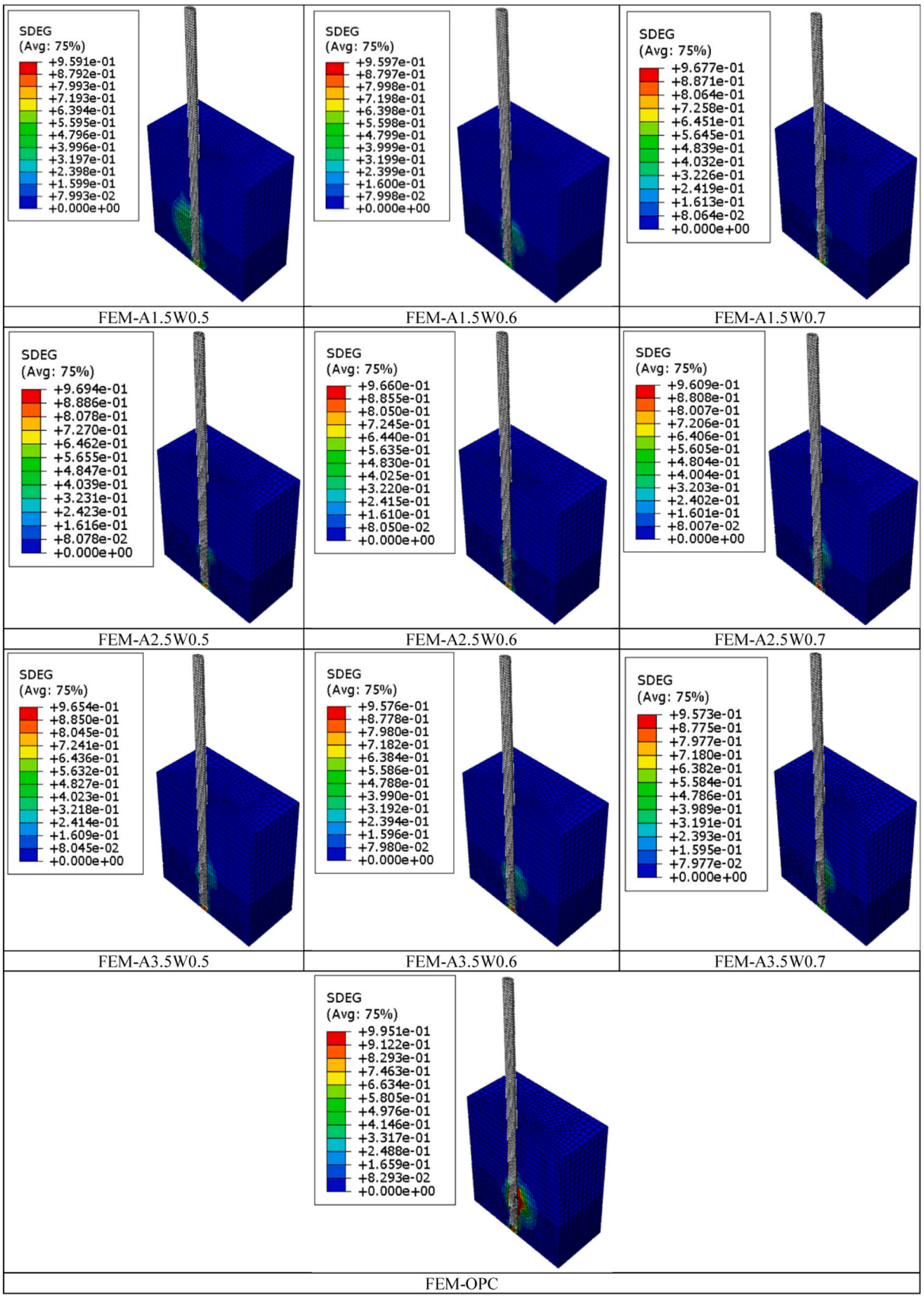

Fig. 24. SDEG views of finite element models (Scalar stifness degradation).

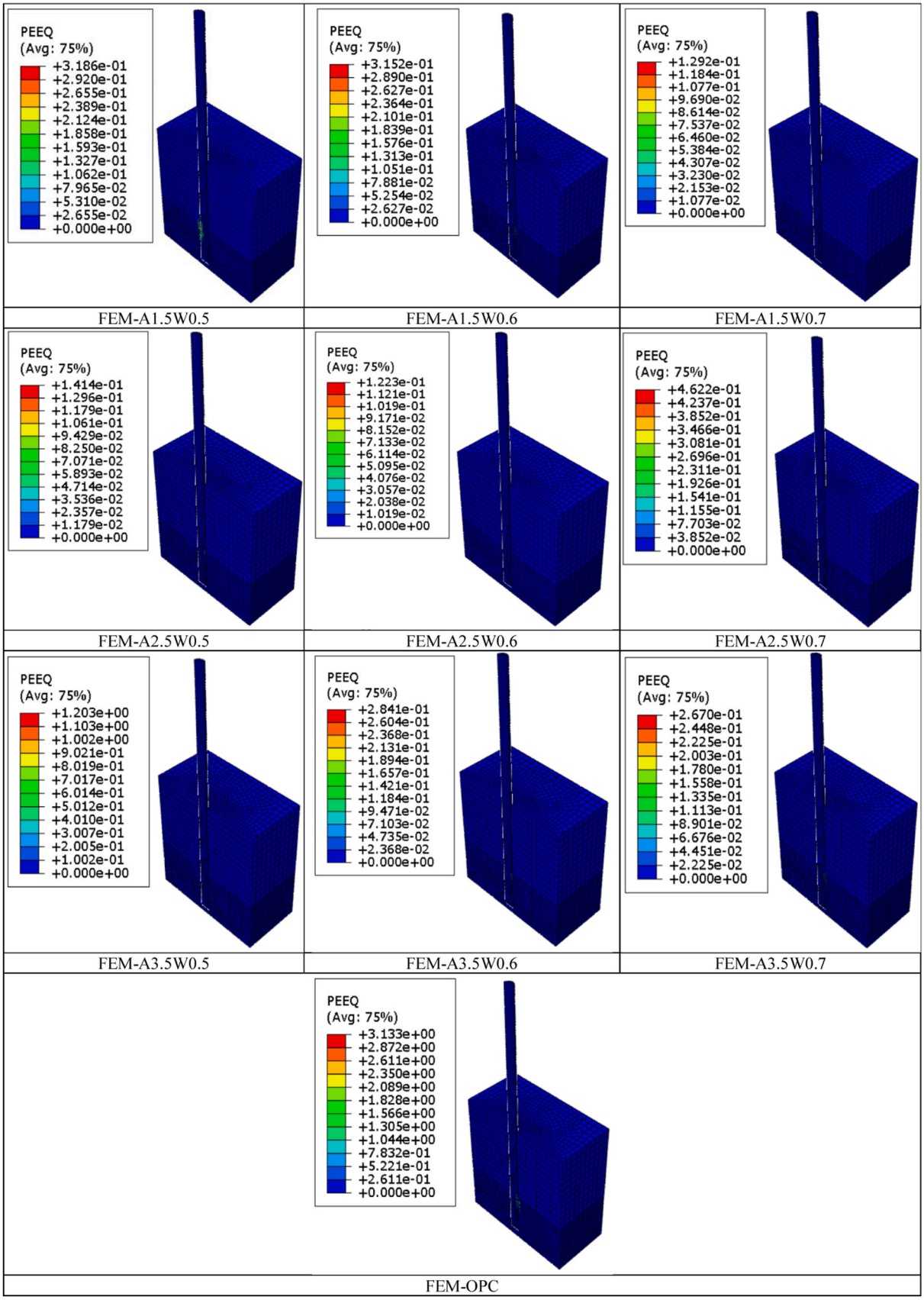

Fig. 25. PEEQ behavior of finite element models (equivalent plastic strain).

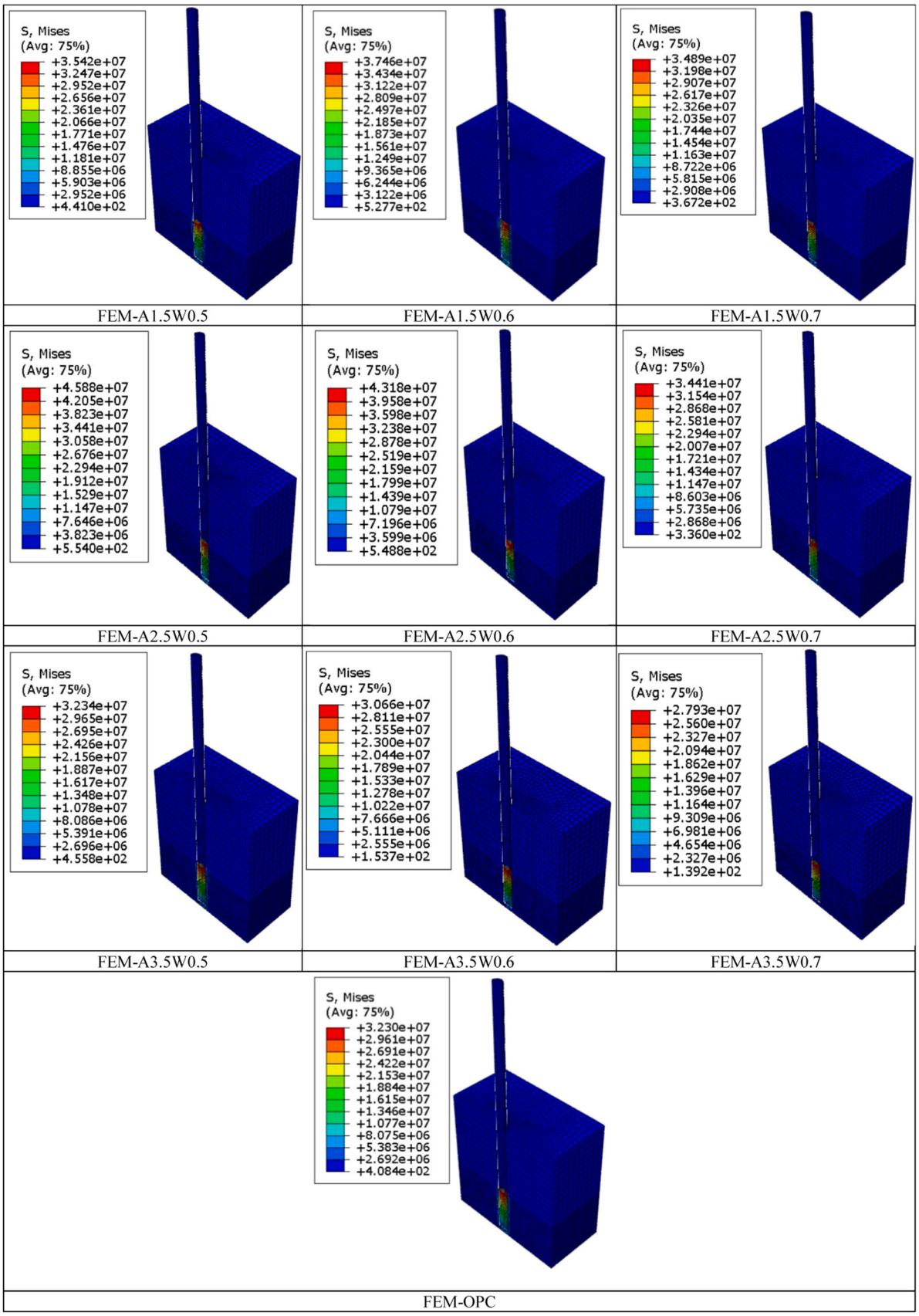

Fig. 26. Stress distribution of finite element models.

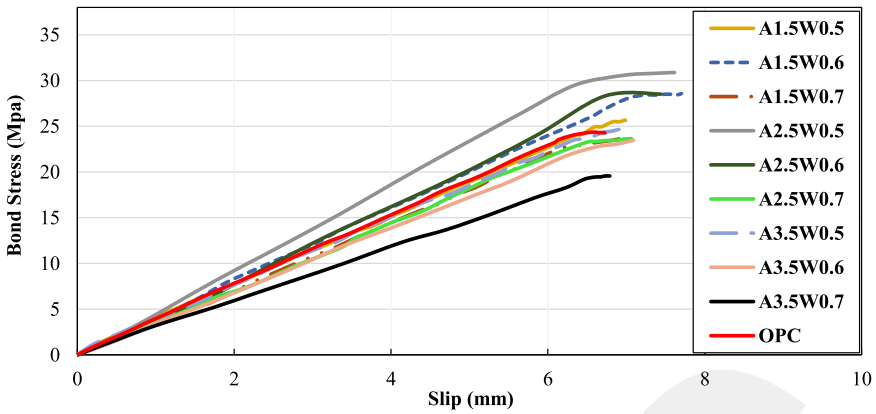

Fig. 27. Bond stress-slip curves obtained from the FE model of adherence samples.

properties based on the level of damage or concentrated plastic deformation. When comparing SDEG views, it was observed that analysis for all specimens was terminated after the yield point. This means that the analyses were completed without experiencing any stiffness loss in the specimens. Therefore, SDEG behaviors are similar for all specimens.

In ABAQUS, Equivalent plastic strain (PEEQ) value was calculated using the Von Mises yield criterion, which is a widely used yield criterion based on the effective stress and strain state of a material. The PEEQ value plays a critical role in analyzing the plastic deformation behavior of the specimen under loading conditions. Equivalent plastic strain values are shown in Fig. 25. The PEEQ value represents the non-elastic deformation of concrete when it undergoes yielding. By comparing PEEQ values, it was observed that geopolymer specimens exhibited lower plastic deformation than OPC specimens. The highest PEEQ values were obtained from the OPC specimens. Due to the lower plastic deformations in geopolymer specimens, having higher bond strengths implies that they are more rigid. By comparing within the geopolymer concrete specimens, it was determined that the specimens with an SS/SH ratio of 2.5 exhibited the lowest PEEQ values. Increasing the AA/FA ratio relatively increased the PEEQ value. Geopolymer specimens exhibiedt convergence in PEEQ values since they reached yield at a similar displacement. An increase in the AA/FA ratio increased the PEEQ value relatively.

As investigated the stress distributions shown in Fig. 26, it was determined that the highest stresses occurred in the A2.5W0.5 and A2.5W0.6 models. The stress behavior of the A1.5 series models was found to be similar to the OPC model. The highest stress distribution occurred in the A2.5W0.5 specimen. Stress values were higher compared to other ratios in samples with an AA/FA ratio of 0.5. Increasing the AA/FA ratio tends to relatively decrease the stress values. While the stress behavior was similar in geopolymer specimens, the stress values significantly decreased in the A3.5W0.7 model.

4.2.2. Numerical bond strength results and comparison the experimental test with the numerical model

The bond stress-slip curves obtained from the load-displacement values by using the finite element models are shown in Fig. 27. Analyses were terminated after the yield load due to excessive deformation in the finite element modeling.

Upon investigating the curves, it was determined that the specimens exhibited similar behavior in terms of slip values. The finite element models were resulted in the highest bond stress value being obtained from the A2.5W0.5 series. The OPC series exhibited similarity with the A1.5 series, while the lowest bond stress value was obtained from the A3.5W0.7 series. Fig. 28 presents the comparative graphs of experimental and finite element-derived bond stress-slip curves up to the yield load. Table 9 provides a comparison between experimental and finite element model results.

As evaluated the results, it was determined that the greatest similarity existed between the experimental and numerical results of the OPC specimens. It was observed that the experimental results aligned with the finite element results in all series. In finite element models, the yield load was between 6–7 mm for all series, while this range was 6–12 mm in experimental studies. The highest bond stress values in the finite element results were obtained from the series with an SS/SH ratio of 2.5. In the experimental studies, all series reached the yield point at similar stress values. Geopolymer specimens exhibited yielding within the range of 23–26 MPa, while OPC specimens yielded between 24–26 MPa. The highest values were obtained from the OPC series by considering the bond stress values at the yield point.

4.3. Evaluation of the comparison of experimental and numerical results

- In the series with SS/SH ratio of 1.5 and 2.5 in the geopolymer adherence samples, the compressive strength, bond load, and bond stress were similar and higher in the series, while in the series with the AA/FA ratio of 0.5, there was a decrease of 34% and 32% compared to the series with 1.5 and 2.5, in the series with AA/FA ratio of 0.5. In the series where it was 0.7, a decrease of 26% and 12% was observed, respectively.
- When the peak load values between GPC and OPC were compared, the average OPC peak load value was calculated as 110.86 kN. The series with a lower average peak load value compared to the OPC average in the GPC series are the A1.5W0.7, A3.5W0.6 and A3.5 W0.7 series. As an inference, it was identified that lower results were obtained from the series with SS/SH= 3.5 and AA/FA of 0.7 compared to OPC. A2.5W0.6 series reached the highest average peak load value and the average load value was 120.6 kN. A load increase of 8.79% was determined compared to the OPC samples.
- In experimental studies, the increase in bond stress value in OPC samples from yield load was 13.58% up to peak load, while the increase trend in geopolymer series was between 10% and 24.45%. The highest percentage of increase belonged to the A2.5W0.6 series with an increase of 24.45%.
- In the finite element models, the highest stress values were obtained from the series with SS/SH= 2.5. A2.5W0.5 series was the sample with the highest stress values. Compared to the OPC sample, 42.04% higher tensile values were measured. The lowest stress values were obtained from the A3.5W0.7 series. Compared to the OPC sample, a lower value of 15.65% was obtained. An increase in the AA/FA ratio decreases the stress value relatively. Increasing the SS/SH ratio from 1.5 to 2.5 creates a positive effect in geopolymer samples, while increasing it to 3.5 creates a negative effect in terms of tensile behavior.
- When the peak load values were compared, it was calculated that in the series where the SS/SH ratio was 1.5, the average load decreased

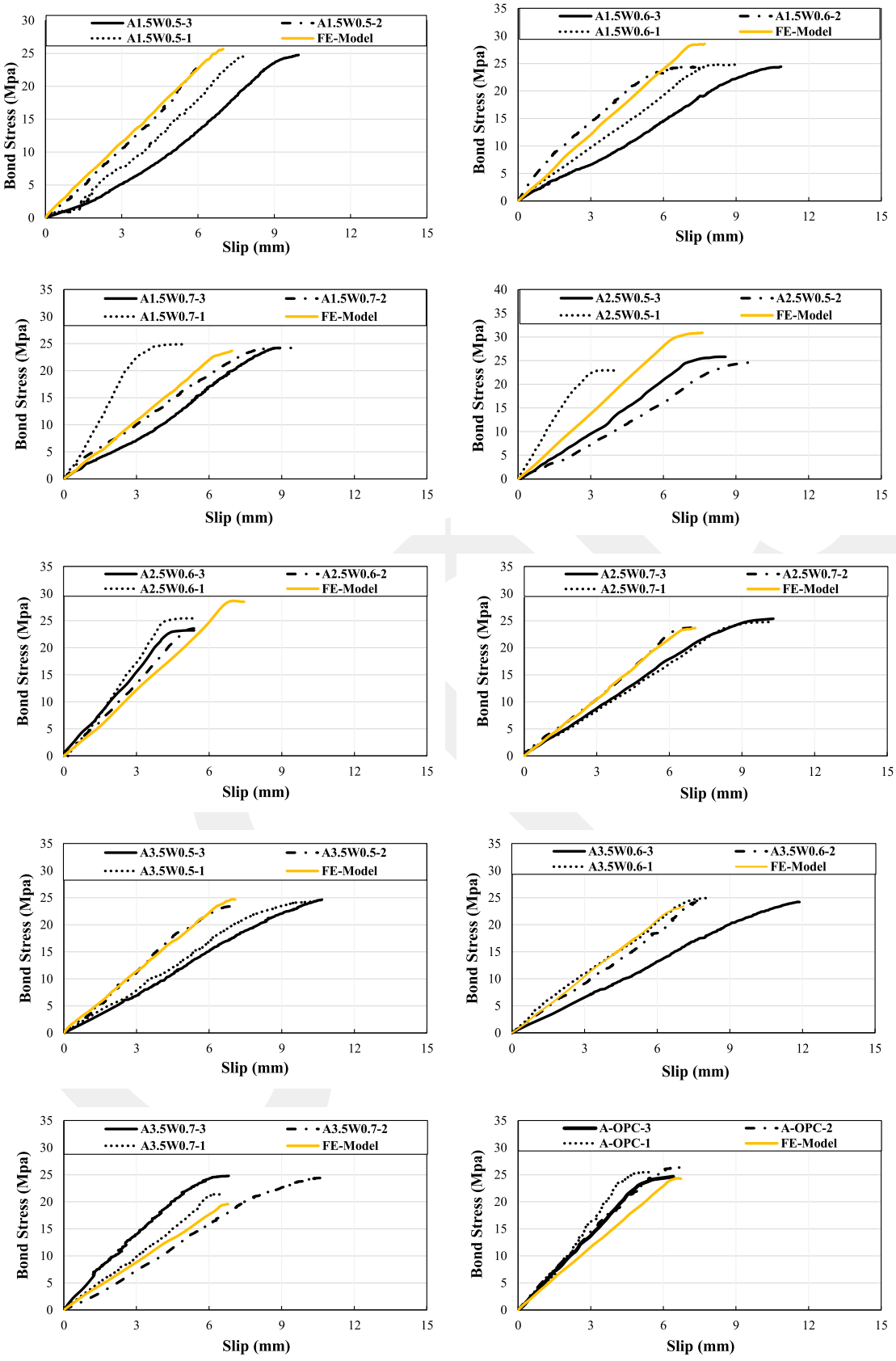

Fig. 28. Comparison of bond stress-slip curves of experimental and numerical results.

by 4.48% by increasing the AA/FA ratio from 0.5 to 0.6, and it decreased by 7% by increasing it to 0.7. In the series with SS/SH=2.5,SS/SH= 2.5, average load increased by 8.52% and 3.36%, respectively.

5. Conclusion

In this study, the adherence between the geopolymer concrete produced by using fly ash and the ribbed reinforcing steel was investigated both experimentally and numerically. For this, a total of 30 samples produced from 27 geopolymer concrete and 3 Ordinary Portland Concrete specimens with different sodium silicate and sodium hydroxide ratios (SS/SH) and alkaline activator and fly ash (AA/FA) ratios were subjected to pull-out test. In addition, the numerical results obtained from the finite element models generated by the ABAQUS were compared with the experimental results obtained. In addition, all the results obtained were compared with the results obtained from ordinary Portland concrete samples. In the light of these data, the following conclusions were obtained.

- Accordingly, while an increase in the SS/SH ratio improves the mechanical properties such as compressive strength and bond load, an increase in the AA/FA ratio causes the opposite effect, especially in the 0.7 series.
- When the failure mode types were evaluated, it was found that the damage mode in the form of shear in the reinforcement was observed in the series with a SS/SH ratio of 1.5, while the damage mode was observed in the form of splitting in the concrete with the increase in the SS/SH ratio. In OPC samples, it was determined that the damage mode occurred in the form of stripping in the reinforcement. Based on this result, it was determined that GPC concrete provides better adherence with reinforcement compared to OPC concrete and its interaction with reinforcement is at a high level.
- Considering the bond stress values at the time of yielding, the highest values were determined in the OPC series, while the highest values were obtained from the geopolymer series when the entire curve until the failure mode was taken into account. This shows that geopolymer concrete increases the maximum stress after yielding as a positive effect.
- In the series with AA/FA ratio of 0.5 and 0.6, it was identified that the bond stress values calculated in the literature showed similar values with the experimental studies.
- When comparing the bond performance of GPC and OPC specimens by investigating the established k/kcc ratios where OPC concrete is taken as a reference, it is observed that geopolymer concrete provides values above 1.00 in nearly all series compared to OPC concrete. This indicates that geopolymer concrete has a more positive effect on adherence.
- In the series with an SS/SH ratio of 1.5, increasing the AA/FA ratio decreases the compressive damage distribution, while in the series with an SS/SH ratio of 3.5, the distribution increases. The series with the least observed compressive damage is the A2.5 series, where the bond loads are calculated to be the highest. OPC specimens exhibit more ductile behavior compared to geopolymer specimens.
- Since the plastic deformations are less in geopolymer concrete samples, it means that the samples are more rigid due to their higher bond strength.
- An increase in NAOH content based on the amount of fly ash in alkali activators adversely affects geopolymerization, leading to a decrease in mechanical properties.

6. Limitation of the study and scope for future studies

This study covers heat-cured fly ash based geopolymer concrete and OPC concretes. In this study, bond strengths were obtained by performing tensile tests on GPC samples with varying sodium silicate/sodium hydroxide (SS/SH) and alkaline activator/fly ash (AA/FA) ratios. While the SS/SH ratio is limited to 1.5, 2.5 and 3.5, the AA/FA ratio is limited to 0.5, 0.6 and 0.7. While compressive strength, adherence strength and bond-slip curves were experimentally targeted within the scope of the research, compressive damage, scalar stiffness degradation (SDEG), equivalent plastic strain (PEEQ) and stress distribution behaviors were examined numerically in addition to the experimental targets within the scope of numerical modeling. In future studies adherence strength of fly ash-based geopolymer concrete can be investigated. Also, the different mix design can be used for the production of the GPC samples by using a different binder material, as well as SS/SH and AA/FA variables in different ratios to investigate the mechanical properties such as bond, adherence and compressive strength. In addition, experimental studies can be investigated numerically, as in this study, to ensure the similarity and overlap between experimental and numerical studies.

CRediT authorship contribution statement

Aslanbay Yuksel Gul: Writing – review & editing, Writing – original draft, Visualization, Validation, Supervision, Software, Project administration, Methodology, Investigation, Formal analysis, Data curation. **Özbayrak Ahmet:** Visualization, Validation, Supervision, Resources, Project administration, Methodology, Investigation, Funding acquisition, Formal analysis, Data curation, Conceptualization. **Aslanbay Huseyin Hilmi:** Writing – review & editing, Writing – original draft, Visualization, Validation, Supervision, Software, Project administration, Methodology, Funding acquisition, Formal analysis, Data curation, Conceptualization. **Atas Oguzhan:** Writing – review & editing, Writing – original draft, Visualization, Methodology, Investigation. **Kucukgoncu Hurmet:** Writing – review & editing, Writing – original draft, Visualization, Project administration, Methodology, Investigation.

Declaration of Competing Interest

The authors declare the following financial interests/personal relationships which may be considered as potential competing interests. AHMET OZBAYRAK reports financial support was provided by TUBITAK The Scientific and Technological Research Council of Türkiye Project Number is 121M236.

Data Availability

Data will be made available on request.

Acknowledgement

This research was supported by TUBITAK (The Scientific and Technological Research Council of Turkey) under grant number 121M236.

References

[1] USGS, Cement Statistics and Information, U.S. Geol. Surv. 53 (2020) 1689–1699. ⟨https://www.usgs.gov/centers/nmic/cement-statistics-and-information⟩ (accessed April 17, 2023).
[2] B. Kanagaraj, N. Anand, A.D. Andrushia, E. Lubloy, Investigation on engineering properties and micro-structure characteristics of low strength and high strength geopolymer composites subjected to standard temperature exposure, Case Stud. Constr. Mater. 17 (2022) e01608, https://doi.org/10.1016/J.CSCM.2022.E01608.
[3] Z.T. Yao, X.S. Ji, P.K. Sarker, J.H. Tang, L.Q. Ge, M.S. Xia, Y.Q. Xi, A comprehensive review on the applications of coal fly ash, Earth-Sci. Rev. 141 (2015) 105–121, https://doi.org/10.1016/J.EARSCIREV.2014.11.016.
[4] A.R.K. Gollakota, V. Volli, C.M. Shu, Progressive utilisation prospects of coal fly ash: a review, Sci. Total Environ. 672 (2019) 951–989, https://doi.org/10.1016/J.SCITOTENV.2019.03.337.
[5] B.C. McLellan, R.P. Williams, J. Lay, A. Van Riessen, G.D. Corder, Costs and carbon emissions for geopolymer pastes in comparison to ordinary portland cement, J. Clean. Prod. 19 (2011) 1080–1090, https://doi.org/10.1016/J.JCLEPRO.2011.02.010.

[6] F. Fan, Z. Liu, G. Xu, H. Peng, C.S. Cai, Mechanical and thermal properties of fly ash based geopolymers, Constr. Build. Mater. 160 (2018) 66–81, https://doi.org/10.1016/J.CONBUILDMAT.2017.11.023.

[7] A. Özbayrak, H. Kucukgoncu, O. Atas, H.H. Aslanbay, Y.G. Aslanbay, F. Altun, Determination of stress-strain relationship based on alkali activator ratios in geopolymer concretes and development of empirical formulations, Structures 48 (2023) 2048–2061, https://doi.org/10.1016/J.ISTRUC.2023.01.104.

[8] A. Özbayrak, H. Kucukgoncu, H.H. Aslanbay, Y.G. Aslanbay, O. Atas, Comprehensive experimental analysis of the effects of elevated temperatures in geopolymer concretes with variable alkali activator ratios, J. Build. Eng. 68 (2023) 106108, https://doi.org/10.1016/J.JOBE.2023.106108.

[9] B.C. Mendes, L.G. Pedroti, C.M.F. Vieira, M. Marvila, A.R.G. Azevedo, J.M. Franco de Carvalho, J.C.L. Ribeiro, Application of eco-friendly alternative activators in alkali-activated materials: a review, J. Build. Eng. 35 (2021) 102010, https://doi.org/10.1016/J.JOBE.2020.102010.

[10] M. Sofi, J.S.J. Van Deventer, P.A. Mendis, G.C. Lukey, Bond performance of reinforcing bars in inorganic polymer concrete (IPC), J. Mater. Sci. 42 (2007) 3107–3116, https://doi.org/10.1007/S10853-006-0534-5.

[11] P. Duxson, A. Fernández-Jiménez, J.L. Provis, G.C. Lukey, A. Palomo, J.S.J. Van Deventer, Geopolymer technology: the current state of the art, J. Mater. Sci. 42 (2007) 2917–2933, https://doi.org/10.1007/S10853-006-0637-Z.

[12] A. Castel, S.J. Foster, Bond strength between blended slag and Class F fly ash geopolymer concrete with steel reinforcement, Cem. Concr. Res. 72 (2015) 48–53, https://doi.org/10.1016/J.CEMCONRES.2015.02.016.

[13] H.Y. Zhang, V. Kodur, B. Wu, J. Yan, Z.S. Yuan, Effect of temperature on bond characteristics of geopolymer concrete, Constr. Build. Mater. 163 (2018) 277–285, https://doi.org/10.1016/J.CONBUILDMAT.2017.12.043.

[14] K.H. Mo, U.J. Alengaram, M.Z. Jumaat, Structural performance of reinforced geopolymer concrete members: a review, Constr. Build. Mater. 120 (2016) 251–264, https://doi.org/10.1016/J.CONBUILDMAT.2016.05.088.

[15] P.K. Sarker, Bond strength of reinforcing steel embedded in fly ash-based geopolymer concrete, Mater. Struct. Constr. 44 (2011) 1021–1030, https://doi.org/10.1617/S11527-010-9683-8.

[16] R.D. Moser, P.G. Allison, B.A. Williams, C.A. Weiss, A.J. Diaz, E.R. Gore, P. G. Malone, Improvement in the geopolymer-to-steel bond using a reactive vitreous enamel coating, Constr. Build. Mater. 49 (2013) 62–69, https://doi.org/10.1016/J.CONBUILDMAT.2013.08.001.

[17] S. Songpiriyakij, T. Pulngern, P. Pungpremtrakul, C. Jaturapitakkul, Anchorage of steel bars in concrete by geopolymer paste, Mater. Des. 32 (2011) 3021–3028, https://doi.org/10.1016/J.MATDES.2011.01.048.

[18] X. Jiang, Y. Zhang, R. Xiao, P. Polaczyk, M. Zhang, W. Hu, Y. Bai, B. Huang, A comparative study on geopolymers synthesized by different classes of fly ash after exposure to elevated temperatures, J. Clean. Prod. 270 (2020) 122500, https://doi.org/10.1016/J.JCLEPRO.2020.122500.

[19] X. Jiang, R. Xiao, M. Zhang, W. Hu, Y. Bai, B. Huang, A laboratory investigation of steel to fly ash-based geopolymer paste bonding behavior after exposure to elevated temperatures, Constr. Build. Mater. 254 (2020) 119267, https://doi.org/10.1016/J.CONBUILDMAT.2020.119267.

[20] A.M. Fernandez-Jimenez, A. Palomo, C. Lopez-Hombrados, Engineering properties of alkali-activated fly ash concrete, ACI Materials Journal 103 (2) (2006) 106.

[21] A. Albidah, A. Altheeb, F. Alrshoudi, A. Abadel, H. Abbas, Y. AI Salloum, Bond performance of GFRP and steel rebars embedded in metakaolin based geopolymer concrete, Structures 27 (2020) 1582–1593, https://doi.org/10.1016/j.istruc.2020.07.048.

[22] G. Trabacchin, W. Sebastian, M. Zhang, Experimental and analytical study of bond between basalt FRP bars and geopolymer concrete, Constr. Build. Mater. 315 (2022) 125461, https://doi.org/10.1016/J.CONBUILDMAT.2021.125461.

[23] B.H. Tekle, A. Khennane, O. Kayali, Bond of spliced GFRP reinforcement bars in alkali activated cement concrete, Eng. Struct. 147 (2017) 740–751, https://doi.org/10.1016/J.ENGSTRUCT.2017.06.040.

[24] N.A. Farhan, M.N. Sheikh, M.N.S. Hadi, Experimental investigation on the effect of corrosion on the bond between reinforcing steel bars and fibre reinforced geopolymer concrete, Structures 14 (2018) 251–261, https://doi.org/10.1016/J.ISTRUC.2018.03.013.

[25] A. Rolland, P. Argoul, K. Benzarti, M. Quiertant, S. Chataigner, A. Khadour, Analytical and numerical modeling of the bond behavior between FRP reinforcing bars and concrete, Constr. Build. Mater. 231 (2020) 117160, https://doi.org/10.1016/J.CONBUILDMAT.2019.117160.

[26] RILEM 7-II-128, RC6: Bond test for reinforcing steel. - Google Akademik, (n.d.). https://scholar.google.com/scholar?q=RILEM 7-II-128, RC6: Bond test for reinforcing steel. 1. Pull-out test, RILEM technical recommendations for the testing and use of construction materials, E FN Spon, London, UK, 1994. (accessed July 15, 2023).

[27] M. Al-Azzawi, T. Yu, M.N.S. Hadi, Factors affecting the bond strength between the Fly Ash-based geopolymer concrete and steel reinforcement, Structures 14 (2018) 262–272, https://doi.org/10.1016/J.ISTRUC.2018.03.010.

[28] N.A. Farhan, M.N. Sheikh, M.N.S. Hadi, Experimental Investigation on the effect of corrosion on the bond between reinforcing steel bars and fibre reinforced geopolymer concrete, Structures 14 (2018) 251–261, https://doi.org/10.1016/J.ISTRUC.2018.03.013.

[29] J. Zhao, G. Cai, J. Yang, Bond-slip behavior and embedment length of reinforcement in high volume fly ash concrete, Mater. Struct. Constr. 49 (2016) 2065–2082, https://doi.org/10.1617/S11527-015-0634-2/FIGURES/12.

[30] P. Topark-Ngarm, P. Chindaprasirt, V. Sata, Setting time, strength, and bond of high-calcium fly ash geopolymer concrete, J. Mater. Civ. Eng. 27 (2014) 04014198, https://doi.org/10.1061/(ASCE)MT.1943-5533.0001157.

[31] P. Zhang, Z. Gao, J. Wang, K. Wang, Numerical modeling of rebar-matrix bond behaviors of nano-SiO2 and PVA fiber reinforced geopolymer composites, Ceram. Int. 47 (2021) 11727–11737, https://doi.org/10.1016/J.CERAMINT.2021.01.012.

[32] B.H. Tekle, A. Khennane, O. Kayali, Bond properties of sand-Coated GFRP bars with fly ash–based geopolymer concrete, J. Compos. Constr. 20 (2016) 04016025, https://doi.org/10.1061/(ASCE)CC.1943-5614.0000685.

[33] Khennane, A., Hailu Tekle, B., Kayali, O., Wales, S., BirukTekle, C., Analytical and finite element modelling of bond behaviour of glass fibre reinforced polymer bars with fly-ash based geopolymer concrete, Researchgate.Net. ,2015. (accessed May 21, 2023).

[34] T.A. Le, T.N. Nguyen, K.T. Nguyen, Experimental, Numerical, and Theoretical Studies of Bond Behavior of Reinforced Fly Ash-Based Geopolymer Concrete, Appl. Sci. 12 (2022), https://doi.org/10.3390/app12157812.

[35] V. Romanazzi, M. Leone, M.A. Aiello, M.R. Pecce, Bond behavior of geopolymer concrete with steel and GFRP bars, Compos. Struct. 300 (2022) 116150, https://doi.org/10.1016/J.COMPSTRUCT.2022.116150.

[36] R.M. Waqas, F. Butt, X. Zhu, T. Jiang, R.F. Tufail, A comprehensive study on the factors affecting the workability and mechanical properties of ambient cured fly ash and slag based geopolymer concrete, 2021, Vol. 11, Page 8722, Appl. Sci. 11 (2021) 8722, https://doi.org/10.3390/APP11188722.

[37] I. Pop, G.De Schutter, P. Desnerck, T. Onet, Bond between powder type self-compacting concrete and steel reinforcement, Constr. Build. Mater. 41 (2013) 824–833, https://doi.org/10.1016/J.CONBUILDMAT.2012.12.029.

[38] H. Abdulrahman, R. Muhamad, P. Visintin, A. Azim Shukri, Mechanical properties and bond stress-slip behaviour of fly ash geopolymer concrete, Constr. Build. Mater. 327 (2022) 126909, https://doi.org/10.1016/J.CONBUILDMAT.2022.126909.

[39] ASTM C618, Standard specification for coal. ASTM Internatıonal, 2005.

[40] ASTM C311, Standard test methods for sampling and testing fly ash or natural pozzolans for use, ASTM Stand. B (04) (2003).

[41] E. Ekinci, İ. Türkmen, Investigation of the effect of different activator and raw material variables on compressive strength of geopolymer paste, Eur. J. Sci. Technol. (2021) 169–175.

[42] M.C.G. Juenger, H.M. Jennings, Effects of high alkalinity on cement pastes, Materials Journal 98 (3) (2001) 251–255.

[43] I. Khan, T. Xu, A. Castel, R.I. Gilbert, M. Babaee, Risk of early age cracking in geopolymer concrete due to restrained shrinkage, Constr. Build. Mater. 229 (2019) 116840, https://doi.org/10.1016/J.CONBUILDMAT.2019.116840.

[44] K. Mermerdaş, S. Manguri, D.E. Nassani, S.M. Oleiwi, Effect of aggregate properties on the mechanical and absorption characteristics of geopolymer mortar, Eng. Sci. Technol. Int. J. 20 (2017) 1642–1652, https://doi.org/10.1016/J.JESTCH.2017.11.009.

[45] ASTM C39, Standard Test Method for Compressive Strength of Cylindrical Concrete Specimens, ASTM Int, West Conshohocken, PA, USA, 2001.

[46] ASTM C469M-14, Standard Test Method for Static Modulus of Elasticity and Poisson's Ratio of Concrete in Compression, ASTM International, 2014.

[47] M. Arezoumandi, M.H. Wolfe, J.S. Volz, A comparative study of the bond strength of reinforcing steel in high-volume fly ash concrete and conventional concrete, Constr. Build. Mater. 40 (2013) 919–924, https://doi.org/10.1016/J.CONBUILDMAT.2012.11.105.

[48] Z. Dahou, A. Castel, A. Noushini, Prediction of the steel-concrete bond strength from the compressive strength of Portland cement and geopolymer concretes, Constr. Build. Mater. 119 (2016) 329–342, https://doi.org/10.1016/J.CONBUILDMAT.2016.05.002.

[49] F. Xu, Z. Wu, J. Zheng, Y. Hu, Q. Li, Experimental Study on the Bond Behavior of Reinforcing Bars Embedded in Concrete Subjected to Lateral Pressure, J. Mater. Civ. Eng. 24 (2011) 125–133, https://doi.org/10.1061/(ASCE)MT.1943-5533.0000365.

[50] Abaqus User's manual Version 6.12 USA Dassault Systemes Simulia Corp, (2012).

[51] K. Cichocki, J. Domski, K. J, M. Ruchwa, Mechanical properties and numerical approach to fibre reinforced WCA concrete slabs, Brittle Matrix Compos (2015) 309–318.

[52] O. Martin, Comparison of different constitutive models for concrete in ABAQUS/explicit for missile impact analyses, JRC Sci. Tech. Rep. (2010).

[53] ABAQUS v 2018., Software Program, Dassault Systemes Simulia Corp.

[54] S.E. Hibbitt H. D, Karlsson B.I., ABAQUS user's manual. Providence (RI): Dassault Systemes Simulia Corp., 2013.

[55] A.Z. Kamali, Shear Strength of Reinforced Concrete Beams subjected to Blast Loading, Royal Institute of Technology (KTH), 2012.

[56] Birtel, V.A.M.P., Mark, P., Parameterised finite element modelling of RC beam shear failure. In *ABAQUS users' conference* (Vol. 14), 2006, May.

[57] W.B. Krätzig, R. Pölling, An elasto-plastic damage model for reinforced concrete with minimum number of material parameters, Computers & structures 82 (15–16) (2004) 1201–1215.

[58] A. Earij, G. Alfano, K.A. Cashell, X. Zhou, Nonlinear three–dimensional finite–element modelling of reinforced–concrete beams: Computational challenges and experimental validation, (2017). ⟨https://bura.brunel.ac.uk/handle/2438/15240⟩ (accessed July 23, 2023).

[59] M. Beliaev, A. Semenov, S. Semenov, A. Benin, Simulation of pulling the reinforcing bar from concrete block with account of friction and concrete damage, In MATEC Web of Conferences, EDP Sciences 73 (2016) 04010, https://doi.org/10.1051/04010.

[60] P.P. Camanho, C.G. D2vila, Mixed-mode decohesion finite elements for the simulation of delamination in composite materials, (2002). ⟨https://ntrs.nasa.gov/citations/20020053651⟩ (accessed July 23, 2023).

[61] B.E. Melnikov, A.S. Semenov, S.G. Semenov, Proc. A.N. Krylov Shipbuild, Res. Inst. 53 (2010) 85–92.
[62] M.A. Sani, R. Muhamad, Bond behaviour of geopolymer concrete in structural application: A review, IOP Conf. Ser.: Earth Environ. 476 (1) (2020) 012017, https://doi.org/10.1088/1755–1315/476/1/012017.
[63] G.B. Maranan, A.C. Manalo, W. Karunasena, B. Benmokrane, Pullout behaviour of GFRP bars with anchor head in geopolymer concrete, Compos. Struct. 132 (2015) 1113–1121, https://doi.org/10.1016/J.COMPSTRUCT.2015.07.021.
[64] Cui, Y., Kayali, O. (2013). Bond performance of steel. https://scholar.google.com/scholar?hl=tr&as_sdt=0%2C5&q=Cui%2C+Y.%2C+Kayali%2C+O.+%282013%29.+Bond+performance+of+steel+bar+and+fly+ash+based&btnG= (accessed April 17, 2023).
[65] J.S. Kim, J.H. Park, An experiment on bond properties of reinforcements embedded in ultra high performance concrete, Mater. Sci. Forum 857 (2016) 323–326, https://doi.org/10.4028/WWW.SCIENTIFIC.NET/MSF.857.323.
[66] C.O. Orangun, J.O. Jirsa, J.E. Breen, A reevaulation of test data on development length and splices, J. Proc. 74 (1977) 114–122, https://doi.org/10.14359/10993.
[67] CEB-FIP, Fib Model Code for Concrete Structures, , 2010.
[68] J. Allen, A. Felder, J. McDermott, A. Azizinamini, Bond and Development of Straight Reinforcing Bars in Tension, (2003). ⟨http://civilwares.free.fr/ACI/MCP04/408r_03.PDF⟩ (accessed December 28, 2023).
[69] A.M. Fernández-Jiménez, A. Palomo, C. López-Hombrados, Engineering properties of alkali-activated fly ash concrete, Acids Mater. J. 103 (2006) 106–112, https://doi.org/10.14359/15261.
[70] N. Ganesan, P.V. Indira, A. Santhakumar, Bond behaviour of reinforcing bars embedded in steel fibre reinforced geopolymer concrete, Https://Doi.Org/10.1680/Macr.14.00125. 67 (2015) 9–16. https://doi.org/10.1680/MACR.14.00125.
[71] B. Tekle, Y. Cui, A. Khennane, Bond properties of steel and sand-coated GFRP bars in Alkali activated cement concrete, Struct Eng Mech. 75 (1) (2020) 123–131. ⟨https://www.dbpia.co.kr/Journal/articleDetail?nodeId=NODE10696731⟩ (accessed December 28, 2023).
[72] S. Qaidi, H.M. Najm, S.M. Abed, H.U. Ahmed, H. Al Dughaishi, J. Al Lawati, M. M. Sabri, F. Alkhatib, A. Milad, Fly ash-based geopolymer composites: a review of the compressive strength and microstructure analysis, 2022, Vol. 15, Page 7098, Materials 15 (2022) 7098, https://doi.org/10.3390/MA15207098.